Acta Neuropathol (2006) 112:681–689
DOI 10.1007/s00401-006-0132-2

ORIGINAL PAPER

α-Synuclein is colocalized with 14-3-3 and synphilin-1 in A53T transgenic mice

Yoshitomo Shirakashi · Yasuhiro Kawamoto · Hidekazu Tomimoto · Ryosuke Takahashi · Masafumi Ihara

Received: 16 May 2006 / Revised: 6 August 2006 / Accepted: 7 August 2006 / Published online: 7 September 2006

Abstract α-Synuclein is a major constituent of Lewy bodies, the neuropathological hallmark of Parkinson's disease (PD). Three types of α-synuclein mutations, A53T, A30P, and E46K, have been reported in familial PD. Wild-type α-synuclein accumulates at high concentrations in Lewy bodies, and this process is accelerated with mutated A53T α-synuclein. The accumulation of α-synuclein is thought to be toxic, and causes neuronal death when α-synuclein aggregates into protofibrils and fibrils. Lewy bodies contain not only α-synuclein, but also other proteins including 14-3-3 proteins and synphilin-1. 14-3-3 Proteins exist mainly as dimers and are related to intracellular signal transduction pathways. Synphilin-1 is known to interact with α-synuclein, promoting the formation of cytoplasmic inclusions like Lewy bodies in vitro. To investigate the colocalization of α-synuclein, synphilin-1, and 14-3-3 proteins, we performed immunohistochemical studies on α-synuclein, 14-3-3 proteins, and synphilin-1 in the brain and spinal cord of A53T transgenic mice. In homozygous mouse brains, α-synuclein immunoreactivity was observed in the neuronal somata and processes in the medial part of the brainstem, deep cerebellar nuclei, and spinal cord. The distribution of 14-3-3 proteins and synphilin-1 immunoreactivity was similar to that of α-synuclein in the homozygous mice. Double immunofluorescent staining showed that α-synuclein and synphilin-1 or 14-3-3 proteins were colocalized in the pons and spinal cord. These results indicate that the accumulation of mutant α-synuclein occurs in association with 14-3-3 proteins and synphilin-1, and may cause the sequestration of important proteins including 14-3-3 proteins and synphilin-1. The sequestration and subsequent decrease in 14-3-3 proteins and synphilin-1 levels may account for neuronal cell death.

Keywords α-Synuclein · A53T transgenic mice · Parkinson's disease · 14-3-3 Proteins · Synphilin-1 · Immunohistochemistry

Y. Shirakashi (✉) · Y. Kawamoto · H. Tomimoto · R. Takahashi · M. Ihara
Department of Neurology, Graduate School of Medicine, Kyoto University, Sakyo-ku, Kyoto 606-8507, Japan
e-mail: yshiraka@kuhp.kyoto-u.ac.jp

M. Ihara
Biochemistry and Cell Biology Unit, Horizontal Medical Research Organization, Graduate School of Medicine, Kyoto University, Sakyo-ku, Kyoto 606-8507, Japan

Introduction

Parkinson's disease (PD), one of the most common neurodegenerative diseases, is characterized neuropathologically by the presence of intracytoplasmic inclusions called Lewy bodies (LBs), which mainly contain aggregated α-synuclein [34]. Point mutations in the α-*Synuclein* genes have been discovered in families afflicted with autosomal dominant inherited PD [23, 28, 38]. α-Synuclein is expressed predominantly in the presynaptic nerve terminals [13]. Under normal conditions, it is thought to have a role in the modulation of synaptic vesicle turnover and synaptic plasticity [6, 8]. However, this physiological role of α-synuclein is not essential for nerve terminal function, because α-synuclein knockout mice display only a mild phenotype. Nevertheless, α-synuclein is likely to protect nerve terminals under

unusual conditions such as neuronal stress or injuries, since the transgenic expression of α-synuclein has been shown to abolish the lethality and neurodegeneration caused by the deletion of cysteine-string protein-α (CSPα), a co-chaperone protein localized in the synaptic vesicles [6]. Therefore, the loss of functional α-synuclein may predispose dopaminergic neurons to oxidative injury or mitochondrial dysfunction.

Lewy bodies also contain other proteins including ubiquitin [25], parkin [33], cytoskeletal proteins like neurofilaments [32], and septins [16], 14-3-3 proteins [22], and synphilin-1 [36]. The 14-3-3 proteins, a family of protein chaperones, are abundant in the brain, comprising approximately 1% of the total brain proteins [5]. 14-3-3 proteins consist of seven different isoforms, named with Greek letters (β, ε, γ, η, σ, θ, ζ) [12]. 14-3-3 proteins exist mainly as homo- or hetero-dimers consisting of ε and ζ, or θ and ζ subunits, and participate in intracellular signal transduction pathways [1].

14-3-3 Proteins are increased in the cerebrospinal fluid from patients with Creutzfeldt-Jakob disease (CJD), and the detection of 14-3-3 proteins is a marker in the pre-mortem diagnosis of CJD [15]. In recent studies, 14-3-3 proteins were found in abnormal pathological structures, including the neurofibrillary tangles in Alzheimer's disease [24], the Pick bodies in Pick's disease [35], the Lewy bodies in Parkinson's disease [22], the Lewy body-like hyaline inclusions in amyotrophic lateral sclerosis [21], the glial cytoplasmic inclusions in multiple system atrophy [20], the nuclear inclusions in spinocerebellar ataxia-1 [7], the prion plaques in sporadic CJD, and the florid plaques in variant CJD [30]. Ostrerova et al. [27] showed that regions of α-synuclein and 14-3-3 proteins share over 40% homology, and bind to each other. These proteins were found to oppositely regulate parkin activity [31], suggesting important roles for 14-3-3 and α-synuclein together with parkin in the pathogenesis of PD.

On the other hand, Engelender et al. [10] identified synphilin-1, a novel protein which also interacts with α-synuclein to form cytoplasmic inclusions in vitro. The C-terminus of synphilin-1 is closely associated with the C-terminus of α-synuclein [19]. The function of synphilin-1 is not fully understood yet; however, it is enriched in the presynaptic terminals, possibly mediating the synaptic function attributed to α-synuclein [29]. Synphilin-1 is enriched in the central cores of LBs, and is presumed to play a role in LB formation in vivo [36]. Recently, Eyal et al. [11] identified synphilin-1A, an isoform of synphilin-1, which has enhanced aggregatory properties and causes neurotoxicity. Synphilin-1A is also observed in LBs. Synphilin-1 and synphilin-1A differ in their exon organization, and are translated from different start codons. Therefore, the N-terminus of synphilin-1A is different from that of synphilin-1. In addition, a mutation of the synphilin-1 gene has been detected in two German PD patients [26]. Collectively, clarifying the roles of α-synuclein, 14-3-3, and synphilin-1 in the process of LB formation may shed some light on the pathogenesis of PD.

In this study, we examined A53T-Tg mice, which overexpress mutated human A53T α-synuclein under the control of a prion promoter, using immunohistochemistry for α-synuclein, the seven 14-3-3 isoforms, and synphilin-1. α-Synuclein has a tendency to self-aggregate and form fibrils in the presence of the familial PD-linked A53T mutation of α-synuclein [9], and the A53T-Tg mice show numerous α-synuclein-based aggregates in the brain [14]. We determined the distribution of the seven 14-3-3 isoforms and synphilin-1 in the aggregates from these mice to uncover the roles of 14-3-3 proteins and synphilin-1 in the pathogenesis of PD.

Materials and methods

Transgenic mice expressing A53T mutant human α-synuclein (A53T-Tg mice)

We used transgenic mice expressing the A53T mutant human α-synuclein (A53T-Tg mice), which were described in a previous paper [14]. In brief, these Tg mice were generated by using the MoPrP. Xho expression vector, which drives the high expression of A53T mutant human α-synuclein in most CNS neurons. Homozygous A53T-Tg mice develop a motor phenotype, but their litter heterozygous A53T-Tg mice show no neurological symptoms or signs, at least before they become 20 months old. We investigated five homozygous A53T-Tg mice and five heterozygous A53T-Tg mice.

Tissues

The A53T-Tg mice were deeply anesthetized with sodium pentobarbital and then perfused transcardially with 0.01 M phosphate-buffered saline (PBS; Nacalai Tesque, Kyoto, Japan), followed by a fixative containing 4% paraformaldehyde and 0.2% picric acid in 0.1 M phosphate buffer (pH 7.4). Following the surgical removal of the brains and spinal cords, the tissues were fixed for 24 h in the same fixatives, and then stored in 20% sucrose in 0.1 M PBS (pH 7.4). The brains and spinal cords were sliced into coronal and axial sections, respectively (20 μm thick) on a cryostat.

Primary antibodies

As the primary antibodies, we used a goat polyclonal anti-α-synuclein antiserum [C-20; Santa Cruz Biotechnology (SCB), diluted 1:500], a rabbit polyclonal anti-α-synuclein antiserum (C-20R; SCB, diluted 1:500), a rabbit polyclonal anti-human synphilin-1 antiserum (Sy-1-C; an antibody to the C-terminal region of synphilin-1, 1:100) [17], a rabbit polyclonal anti-ubiquitin antiserum (U5379; SIGMA, diluted 1:1,000), and several types of anti-14-3-3 antibodies: a rabbit polyclonal anti-14-3-3β antiserum (C-20; SCB, diluted 1:2,000), a goat polyclonal anti-14-3-3β antiserum (A-15; SCB, diluted 1:1,000), a rabbit polyclonal anti-14-3-3γ antiserum (C-16; SCB, diluted 1:2,000), a rabbit polyclonal anti-14-3-3ζ antiserum (C-16; SCB, diluted 1:2,000), a rabbit polyclonal anti-14-3-3θ antiserum (C-17; SCB, diluted 1:2,000), a rabbit polyclonal anti-14-3-3ε antiserum (T-16; SCB, diluted 1:400), a goat polyclonal anti-14-3-3η antiserum (E-12:SCB, diluted 1:400), a goat polyclonal anti-14-3-3σ antiserum (C-18, against the C-terminus of 14-3-3σ; SCB, diluted 1:400), and a goat polyclonal anti-14-3-3σ antiserum (N-14, against the N-terminus of 14-3-3σ; SCB, diluted 1:400).

Immunohistochemistry

The brain and spinal cord sections were incubated with the primary antibodies in 0.1 M PBS overnight at 4 C. Subsequently, these sections were treated with the appropriate biotinylated secondary antibodies (diluted 1:200; Vector Laboratories, Burlingame, CA, USA) for 1 h at room temperature, followed by an incubation with an avidin–biotin–peroxidase complex (ABC) kit (Vector) diluted in 0.1 M PBS (1:200) for 1 h at room temperature. The sections were visualized with 0.01% diaminobenzidine tetrahydrochloride (DAB; Dojin, Kumamoto, Japan), and 0.005% H_2O_2 in 0.05 M Tris–HCl (pH 7.6) for 10 min at room temperature. Adjoining sections were used for the immunohistochemical investigation of α-synuclein, synphilin-1, and 14-3-3 proteins in the brain and the spinal cord.

Double labeling immunohistochemistry

To investigate the relationship between α-synuclein and 14-3-3 proteins or synphilin-1, the brain sections were incubated with primary antibodies raised against α-synuclein and 14-3-3 or synphilin-1, followed by immunofluorescent staining procedures with fluorescein isothiocyanate-conjugated swine anti-goat immunoglobulins (ACI0408; Biosource) and tetramethylrhodamine-conjugated swine anti-rabbit immunoglobulins (R0156; DAKO).

Results

Distribution of α-synuclein immunoreactivity

In the homozygous mouse brains, α-synuclein immunoreactivity was observed in the neuronal somata and processes. Some α-synuclein immunoreactivity in the somatodendritic compartment appeared as LB-like inclusions. These α-synuclein immunoreactive granules were abundant in the medial part of the midbrain and pons (Figs. 1a, 4), deep cerebellar nuclei (DCN) (Fig. 1b), and spinal cord (Fig. 1c). In these areas, a similar immunolabeling pattern was also observed for ubiquitin (Fig. 1e–g). In age-matched litter heterozygous mouse brains, however, immunostaining for α-synuclein was observed in the neuropil, without any immunostaining in the somatodendritic compartment (Fig. 1d).

Synphilin-1 immunoreactivity

Immunoreactivity for synphilin-1 in the homozygous mice was observed in the somatodendritic compartment of the pons (Fig. 2a), DCN (Fig. 2b) and spinal cord (Fig. 2c). There was no immunoreactivity for synphilin-1 in the axons. In the heterozygous mouse brains, no or faint immunoreactivity for synphilin-1 was detected (Fig. 2d).

14-3-3 Protein immunoreactivity

In the homozygous mice, immunoreactivity for 14-3-3ζ was observed mainly in the somatodendritic compartment in the medial part of the brainstem, motor cortex, and caudoputamen; however, faint immunoreactivity was detected in the spinal cord. 14-3-3ζ immunoreactivity in the heterozygous mice was observed mainly in the cerebral cortex and caudoputamen, but was not detected in the pons (Fig. 2e). Immunoreactivity for 14-3-3β, γ, and θ in the homozygous mouse brains was found mainly in the somatodendritic compartment of the pons, and spinal cord (Fig. 2f, g). In the heterozygous mice, immunoreactivity for 14-3-3β (C-20), γ, and θ was positive in the cerebral cortex, pons, and deep cerebellar nucleus, but there was no or faint immunoreactivity in the spinal cord (Fig. 2h). In the heterozygous mice, immunoreactivity for 14-3-3β (A-15) was also observed in the cerebral cortex, pons, deep cerebellar nucleus, and spinal cord. However, in the

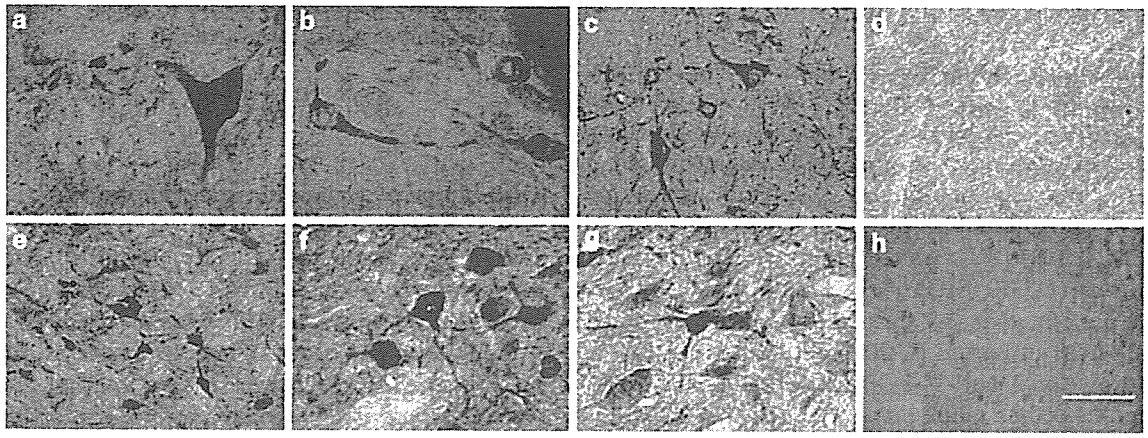

Fig. 1 Immunostaining for α-synuclein (**a–d**) and ubiquitin (**e–h**) in homozygous mice (**a–c**, **e–g**) and heterozygous mice (**d**, **h**). The photomicrographs were taken from the pons (**a**, **e**), deep cerebellar nucleus (**b**, **f**), and cervical spinal cord (**c**, **d**, **g**, **h**). Strong immunoreactivity for α-synuclein and ubiquitin was observed in the somatodendritic compartment in the pons, deep cerebellar nucleus, and cervical cord in the homozygous mice. In the heterozygous mice, no or faint immunoreactivity was observed in the somatodendritic compartment (**d**, **h**). *Scale bar* 50 μm (**a–c**, **f**, **g**), 100 μm (**d**, **e**, **h**)

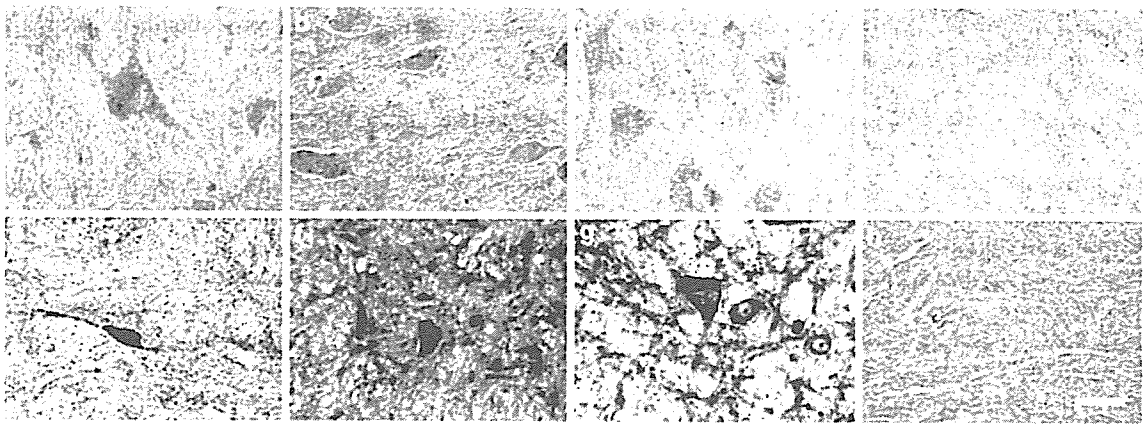

Fig. 2 Immunostaining for synphilin-1 (**a–d**) and 14-3-3 [**e–h**; **e** 14-3-3ζ, **f** 14-3-3β (A-15), **g–h** 14-3-3γ] in homozygous mice (**a–c**, **e–g**) and heterozygous mice (**d**, **h**). The photomicrographs were taken from the pons (**a**, **e**), deep cerebellar nucleus (**b**), lumbar spinal cord (**f**), and cervical spinal cord (**c**, **d**, **g**, **h**). Strong immunoreactivity for synphilin-1, 14-3-3ζ, 14-3-3β, and 14-3-3γ was observed in the somatodendritic compartment in the pons, deep cerebellar nucleus, and spinal cord in the homozygous mice. In the heterozygous mice, no or faint immunoreactivity was observed in the somatodendritic compartment (**d**, **h**). *Scale bar* 50 μm (**a–c**, **e–g**), 100 μm (**d**, **h**)

homozygous mice, strong 14-3-3β (A-15) immunoreactivity was observed in the granules of the neuronal somata and dendrites (Fig. 2f). Immunoreactivity for 14-3-3ε in the homozygous mice was localized to the neuronal nuclei in the cerebral cortex, brainstem, deep cerebellar nuclei, and spinal cord. In the heterozygous mice, 14-3-3ε immunoreactivity was observed also in the same areas as the homozygous mice, except for the spinal cord.

Immunoreactivity for 14-3-3η and σ in the homozygous mice was localized to the neuronal somatodendritic components in the cerebral cortex, brainstem, deep cerebellar nuclei, and spinal cord. Immunoreactivity for 14-3-3η and σ in the heterozygous mice was also observed in the same areas as the homozygous mice, and there were no remarkable differences in the distribution of 14-3-3η and σ between the homozygous and heterozygous mice.

Double immunofluorescent staining

In the homozygous mice, the distribution of immunoreactivity for synphilin-1 and 14-3-3 was mainly observed in the medial part of the midbrain and pons, DCN, and spinal cord, and was similar to that of α-synuclein (Fig. 4).

Double-immunofluorescent-stained sections in the homozygous mice showed that 14-3-3β and γ were colocalized with α-synuclein in the spinal cord. 14-3-3ζ was colocalized with α-synuclein in the pons. Synphilin-1 was also colocalized with α-synuclein in the pons (Fig. 3). By randomly sampling three arbitrary regions in the pons, the mean frequencies of double labeling for 14-3-3β, γ, θ, ζ, and ε immunoreactivities with α-synuclein were 83, 70, 66, 44, and 56%, respectively, in the homozygous mice.

Discussion

The most notable finding of this study using the A53T-Tg mice was that α-synuclein overexpression alone was enough to induce aggregates containing α-synuclein, 14-3-3 proteins, and synphilin-1, which are partially reminiscent of LBs. Given the fact that the difference between homozygous and heterozygous A53T-Tg mice is limited to the magnitude of expression of the transgene-derived human α-synuclein, and that the expres-

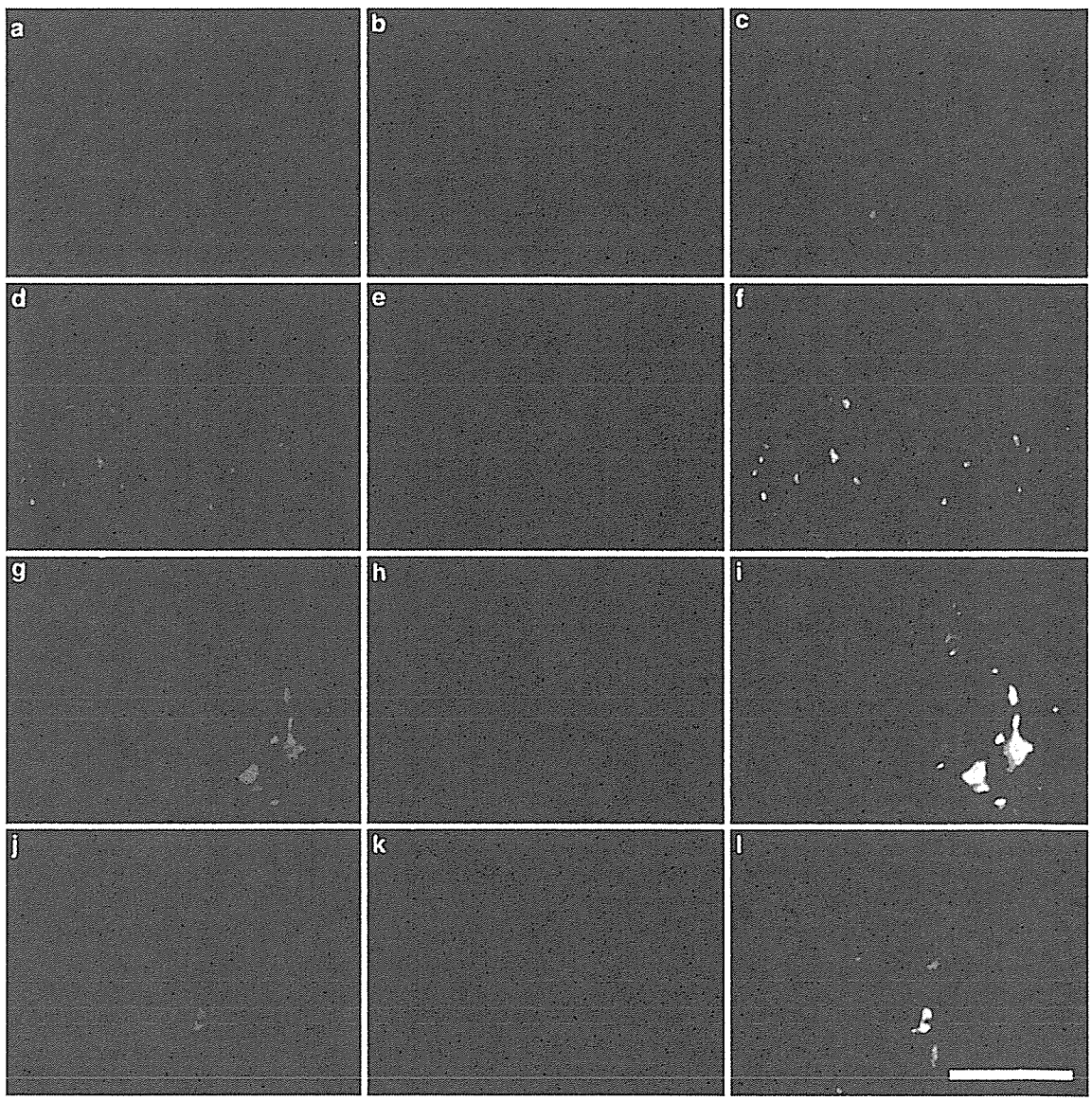

Fig. 3 Double immunofluorescent staining for α-synuclein plus synphilin-1 (**a–c**), and α-synuclein plus 14-3-3 (**d-l**) in homozygous mice. **a–f** pons; **g–i** lumbar spinal cord; and **j–l** thoracic spinal cord. The *left column* (**a**, **d**, **g**, **j**; *green*) shows immunostaining for α-synuclein, and the *middle column* shows (**b**, **e**, **h**, **k**; *red*) immunostaining for synphilin-1 (**b**), 14-3-3ζ (**e**), 14-3-3γ (**h**), and 14-3-3β (**k**). The *right column* (**c**, **f**, **i**, **l**) shows the merged image. *Scale bar* 50 μm (**a–c**), 100 μm (**d–l**)

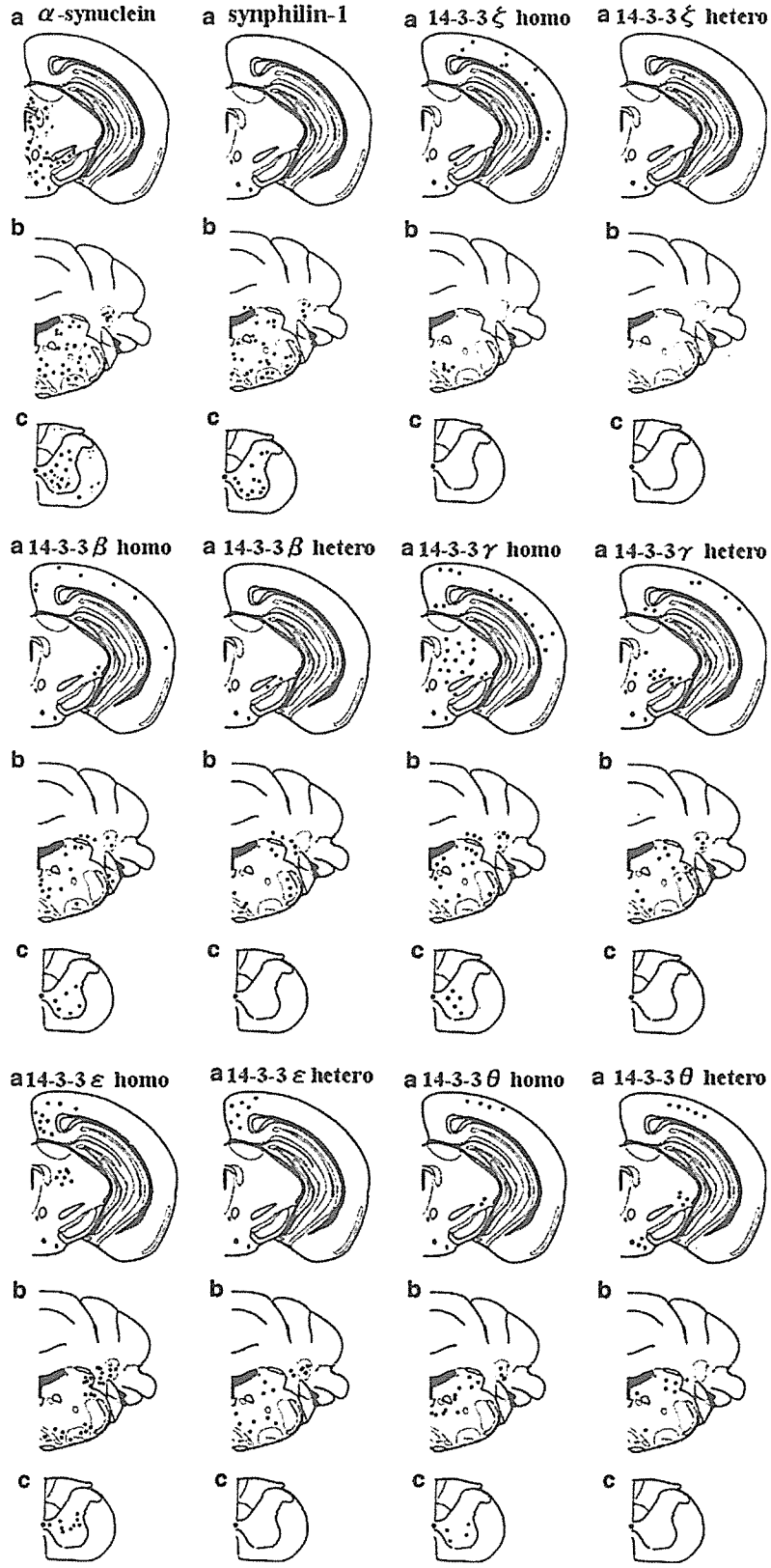

Fig. 4 Schematic distribution of α-synuclein (*α-syn*), synphilin-1 (*sph*), and 14-3-3 in A53T-Tg mice. A schematic summary of the α-synuclein, synphilin-1, and 14-3-3 pathology was shown as coronal sections from the A53T-Tg mouse brain and spinal cord, at the level of the midbrain (**a**), pons and deep cerebellar nucleus (**b**), and the cervical spinal cord (**c**). The *dots* represent one to three neurons with immunoreactivity for each antigen

sion level is approximately 20× higher than the endogenous expression observed in homozygous A53T-Tg mice [14], 14-3-3 proteins and synphilin-1 are more likely to be sequestered into the aggregates, rather than stoichiometrically associated with α-synuclein to form insoluble complexes. The sequestration of 14-3-3 proteins and synphilin-1 into aggregates may decrease the amount of functional 14-3-3 proteins and synphilin-1 available in the synaptic terminal, possibly disrupting chaperone and synaptic functions, respectively.

Under normal conditions, α-synuclein exists as a relatively unfolded molecule in the presynaptic terminals. However, under pathological conditions, it forms fibrils, accumulates in the neuronal somata, and may form inclusion bodies. In the heterozygous mice, α-synuclein has been reported to exhibit a neuropil immunostaining pattern [14], and this study showed a similar result without any immunoreactivities for α-synuclein in the somatodendritic compartment. Immunoreactivities for 14-3-3β and γ in the normal mouse brain have been localized to neurons in the brainstem and cerebral cortex, but not in the spinal cord [3]. These immunostaining patterns were similar in the heterozygous mice, in which the neuronal immunolabeling for 14-3-3β and γ occurred in the brainstem and cerebral cortex. In contrast, in the homozygous mice, 14-3-3γ accumulated in the spinal anterior horn cells (Fig. 4).

The immunostaining patterns for 14-3-3β in the homozygous mice have been strongly positive in the granules from the neuronal somata and dendrites in the spinal cord. The homozygous mice have been shown to develop motor impairments, possibly due to a degeneration of the anterior horn cells. Therefore, this accumulation of 14-3-3β and γ in the anterior horn cell bodies may play a significant role in the development of motor symptoms in these mice. Previously, we showed that LB-like hyaline inclusions in the anterior horn cells were immunoreactive for several 14-3-3 proteins in patients with amyotrophic lateral sclerosis [21]. Taken together, the accumulation of 14-3-3 proteins in the somatodendritic compartments of the anterior horn cells may be generally associated with a dysfunction of the lower motor neurons.

Synphilin-1A, an isoform of synphilin-1, is localized to the LBs and is an aggregation-prone protein that causes neuronal toxicity [11]. In this study, we used an anti-synphilin-1 antibody which recognizes the C-terminus of synphilin-1, and thus there was the possibility that this anti-synphilin-1 antibody may have cross-reacted, and showed the localization of synphilin-1A in the homozygous mice. Increasing evidence further supplements the conjugation of α-synuclein with 14-3-3 proteins or synphilin-1. In cell cultures, the co-transfection of synphilin-1 and α-synuclein has been shown to promote the formation of eosinophilic cytoplasmic inclusions like LBs [10]. Xu and colleagues [37] showed that soluble wild-type and mutant α-synuclein form complexes with 14-3-3 proteins, and accumulate in dopaminergic neurons. The colocalization of 14-3-3 proteins or synphilin-1 with α-synuclein in LBs has been demonstrated in human brains [22, 36]. Under non-pathological conditions, 14-3-3 proteins inhibit apoptosis by binding and inactivating pro-apoptotic proteins, including the mitochondrial Bcl-2 family member BAD and the transcription factor Forkhead [39]. Berg et al. [4] showed that 14-3-3 proteins, especially the ε, γ, θ, and ζ isoforms, were colocalized in the LBs. Kaneko and Hachiya [18] proposed the possibility that the distinctive function of 14-3-3ζ might be a sweeper of misfolded proteins such as aggregates or inclusion bodies. In our study, enhanced immunoreactivity for 14-3-3 proteins and synphilin-1 was observed in the A53T-Tg homozygous mice. According to these results, the 14-3-3 proteins bound to the overexpressed α-synuclein, and thus forming complexes of these proteins which may lead to the sequestration and subsequent decrease in 14-3-3 proteins. In turn, this decrease in 14-3-3 proteins causes the apoptotic neuronal cell death. Furthermore, those 14-3-3 proteins which interact with α-synuclein and accumulate in LBs may also interact with synphilin-1 [2]. The sequestration of synphilin-1 may also contribute to neuronal dysfunction, possibly through an impairment of synaptic function attributed to α-synuclein, although the exact role of synphilin-1 remains to be fully understood. The present study showed that α-synuclein colocalized with 14-3-3 proteins and synphilin-1, suggesting that these multi-protein complexes formed by α-synuclein, synphilin-1, and 14-3-3 proteins may account for the pathogenesis of neuronal cell death.

Acknowledgments We are grateful to Prof. V. M. Lee (Department of Pathology and Laboratory Medicine, University of Pennsylvania) for providing the A53T-Tg mice, and to Prof. E. Iseki (Department of Psychiatry, Juntendo University School of Medicine) for providing the anti-synphilin-1 antibodies.

References

1. Aitken A (1996) 14-3-3 and its possible role in co-ordinating multiple signalling pathways. Trends Cell Biol 6:341–347
2. Avraham E, Szargel R, Eyal A, Rott R, Engelender S (2005) Glycogen synthase kinase 3beta modulates synphilin-1 ubiquitylation and cellular inclusion formation by SIAH: implications for proteasomal function and Lewy body formation. J Biol Chem 280:42877–42886

3. Baxter HC, Liu WG, Forster JL, Aitken A, Fraser JR (2002) Immunolocalisation of 14-3-3 isoforms in normal and scrapie-infected murine brain. Neuroscience 109:5–14
4. Berg D, Riess O, Bornemann A (2003) Specification of 14-3-3 proteins in Lewy bodies. Ann Neurol 54:135
5. Boston PF, Jackson P, Thompson RJ (1982) Human 14-3-3 protein: radioimmunoassay, tissue distribution, and cerebrospinal fluid levels in patients with neurological disorders. J Neurochem 38:1475–1482
6. Chandra S, Gallardo G, Fernandez-Chacon R, Schluter OM, Sudhof TC (2005) Alpha-synuclein cooperates with CSPalpha in preventing neurodegeneration. Cell 123:383–396
7. Chen HK, Fernandez-Funez P, Acevedo SF, Lam YC, Kaytor MD, Fernandez MH, Aitken A, Skoulakis EM, Orr HT, Botas J, Zoghbi HY (2003) Interaction of Akt-phosphorylated ataxin-1 with 14-3-3 mediates neurodegeneration in spinocerebellar ataxia type 1. Cell 113:457–468
8. Clayton DF, George JM (1999) Synucleins in synaptic plasticity and neurodegenerative disorders. J Neurosci Res 58:120–129
9. Conway KA, Harper JD, Lansbury PT (1998) Accelerated in vitro fibril formation by a mutant alpha-synuclein linked to early-onset Parkinson disease. Nat Med 4:1318–1320
10. Engelender S, Kaminsky Z, Guo X, Sharp AH, Amaravi RK, Kleiderlein JJ, Margolis RL, Troncoso JC, Lanahan AA, Worley PF, Dawson VL, Dawson TM, Ross CA (1999) Synphilin-1 associates with alpha-synuclein and promotes the formation of cytosolic inclusions. Nat Genet 22:110–114
11. Eyal A, Szargel R, Avraham E, Liani E, Haskin J, Rott R, Engelender S (2006) Synphilin-1A: an aggregation-prone isoform of synphilin-1 that causes neuronal death and is present in aggregates from alpha-synucleinopathy patients. Proc Natl Acad Sci USA 103:5917–5922
12. Fu H, Subramanian RR, Masters SC (2000) 14-3-3 proteins: structure, function, and regulation. Annu Rev Pharmacol Toxicol 40:617–647
13. George JM, Jin H, Woods WS, Clayton DF (1995) Characterization of a novel protein regulated during the critical period for song learning in the zebra finch. Neuron 15:361–372
14. Giasson BI, Duda JE, Quinn SM, Zhang B, Trojanowski JQ, Lee VM (2002) Neuronal alpha-synucleinopathy with severe movement disorder in mice expressing A53T human alpha-synuclein. Neuron 34:521–533
15. Hsich G, Kenney K, Gibbs CJ, Lee KH, Harrington MG (1996) The 14-3-3 brain protein in cerebrospinal fluid as a marker for transmissible spongiform encephalopathies. N Engl J Med 335:924–930
16. Ihara M, Tomimoto H, Kitayama H, Morioka Y, Akiguchi I, Shibasaki H, Noda M, Kinoshita M (2003) Association of the cytoskeletal GTP-binding protein Sept4/H5 with cytoplasmic inclusions found in Parkinson's disease and other synucleinopathies. J Biol Chem 278:24095–24102
17. Iseki E, Takayama N, Furukawa Y, Marui W, Nakai T, Miura S, Ueda K, Kosaka K (2002) Immunohistochemical study of synphilin-1 in brains of patients with dementia with Lewy bodies - synphilin-1 is non-specifically implicated in the formation of different neuronal cytoskeletal inclusions. Neurosci Lett 326:211–215
18. Kaneko K, Hachiya NS (2006) The alternative role of 14-3-3 zeta as a sweeper of misfolded proteins in disease conditions. Med Hypotheses 67:169–171
19. Kawamata H, McLean PJ, Sharma N, Hyman BT (2001) Interaction of alpha-synuclein and synphilin-1: effect of Parkinson's disease-associated mutations. J Neurochem 77:929–934
20. Kawamoto Y, Akiguchi I, Nakamura S, Budka H (2002) Accumulation of 14-3-3 proteins in glial cytoplasmic inclusions in multiple system atrophy. Ann Neurol 52:722–731
21. Kawamoto Y, Akiguchi I, Nakamura S, Budka H (2004) 14-3-3 proteins in Lewy body-like hyaline inclusions in patients with sporadic amyotrophic lateral sclerosis. Acta Neuropathol (Berl) 108:531–537
22. Kawamoto Y, Akiguchi I, Nakamura S, Honjyo Y, Shibasaki H, Budka H (2002) 14-3-3 proteins in Lewy bodies in Parkinson disease and diffuse Lewy body disease brains. J Neuropathol Exp Neurol 61:245–253
23. Kruger R, Kuhn W, Muller T, Woitalla D, Graeber M, Kosel S, Przuntek H, Epplen JT, Schols L, Riess O (1998) Ala30Pro mutation in the gene encoding alpha-synuclein in Parkinson's disease. Nat Genet 18:106–108
24. Layfield R, Fergusson J, Aitken A, Lowe J, Landon M, Mayer RJ (1996) Neurofibrillary tangles of Alzheimer's disease brains contain 14-3-3 proteins. Neurosci Lett 209:57–60
25. Lowe J, Blanchard A, Morrell K, Lennox G, Reynolds L, Billett M, Landon M, Mayer RJ (1988) Ubiquitin is a common factor in intermediate filament inclusion bodies of diverse type in man, including those of Parkinson's disease, Pick's disease, and Alzheimer's disease, as well as Rosenthal fibres in cerebellar astrocytomas, cytoplasmic bodies in muscle, and mallory bodies in alcoholic liver disease. J Pathol 155:9–15
26. Marx FP, Holzmann C, Strauss KM, Li L, Eberhardt O, Gerhardt E, Cookson MR, Hernandez D, Farrer MJ, Kachergus J, Engelender S, Ross CA, Berger K, Schols L, Schulz JB, Riess O, Kruger R (2003) Identification and functional characterization of a novel R621C mutation in the synphilin-1 gene in Parkinson's disease. Hum Mol Genet 12:1223–1231
27. Ostrerova N, Petrucelli L, Farrer M, Mehta N, Choi P, Hardy J, Wolozin B (1999) alpha-Synuclein shares physical and functional homology with 14-3-3 proteins. J Neurosci 19:5782–5791
28. Polymeropoulos MH, Lavedan C, Leroy E, Ide SE, Dehejia A, Dutra A, Pike B, Root H, Rubenstein J, Boyer R, Stenroos ES, Chandrasekharappa S, Athanassiadou A, Papapetropoulos T, Johnson WG, Lazzarini AM, Duvoisin RC, Di Iorio G, Golbe LI, Nussbaum RL (1997) Mutation in the alpha-synuclein gene identified in families with Parkinson's disease. Science 276:2045–2047
29. Ribeiro CS, Carneiro K, Ross CA, Menezes JR, Engelender S (2002) Synphilin-1 is developmentally localized to synaptic terminals, and its association with synaptic vesicles is modulated by alpha-synuclein. J Biol Chem 277:23927–23933
30. Richard M, Biacabe AG, Streichenberger N, Ironside JW, Mohr M, Kopp N, Perret-Liaudet A (2003) Immunohistochemical localization of 14.3.3 zeta protein in amyloid plaques in human spongiform encephalopathies. Acta Neuropathol (Berl) 105:296–302
31. Sato S, Chiba T, Sakata E, Kato K, Mizuno Y, Hattori N, Tanaka K (2006) 14-3-3eta is a novel regulator of parkin ubiquitin ligase. Embo J 25:211–221
32. Schmidt ML, Murray J, Lee VM, Hill WD, Wertkin A, Trojanowski JQ (1991) Epitope map of neurofilament protein domains in cortical and peripheral nervous system Lewy bodies. Am J Pathol 139:53–65
33. Shimura H, Schlossmacher MG, Hattori N, Frosch MP, Trockenbacher A, Schneider R, Mizuno Y, Kosik KS, Selkoe DJ (2001) Ubiquitination of a new form of alpha-synuclein by parkin from human brain: implications for Parkinson's disease. Science 293:263–269
34. Spillantini MG, Schmidt ML, Lee VM, Trojanowski JQ, Jakes R, Goedert M (1997) Alpha-synuclein in Lewy bodies. Nature 388:839–840

35. Umahara T, Uchihara T, Tsuchiya K, Nakamura A, Ikeda K, Iwamoto T, Takasaki M (2004) Immunolocalization of 14-3-3 isoforms in brains with Pick body disease. Neurosci Lett 371:215–219
36. Wakabayashi K, Engelender S, Yoshimoto M, Tsuji S, Ross CA, Takahashi H (2000) Synphilin-1 is present in Lewy bodies in Parkinson's disease. Ann Neurol 47:521–523
37. Xu J, Kao SY, Lee FJ, Song W, Jin LW, Yankner BA (2002) Dopamine-dependent neurotoxicity of alpha-synuclein: a mechanism for selective neurodegeneration in Parkinson disease. Nat Med 8:600–606
38. Zarranz JJ, Alegre J, Gomez-Esteban JC, Lezcano E, Ros R, Ampuero I, Vidal L, Hoenicka J, Rodriguez O, Atares B, Llorens V, Gomez Tortosa E, del Ser T, Munoz DG, de Yebenes JG (2004) The new mutation, E46K, of alpha-synuclein causes Parkinson and Lewy body dementia. Ann Neurol 55:164–173
39. Zha J, Harada H, Yang E, Jockel J, Korsmeyer SJ (1996) Serine phosphorylation of death agonist BAD in response to survival factor results in binding to 14-3-3 not BCL-X(L). Cell 87:619–628

Matrix Metalloproteinase-2 Plays a Critical Role in the Pathogenesis of White Matter Lesions After Chronic Cerebral Hypoperfusion in Rodents

Kayoko Nakaji, MD; Masafumi Ihara, MD; Chiaki Takahashi, MD; Shigeyoshi Itohara, PhD; Makoto Noda, PhD; Ryosuke Takahashi, MD; Hidekazu Tomimoto, MD

Background and Purpose—Cerebrovascular white matter (WM) lesions contribute to cognitive impairment and motor dysfunction in the elderly. A disruption of the blood–brain barrier (BBB) is believed to be a critical early event leading to these WM lesions. Previous studies have suggested the involvement of matrix metalloproteinase-2 (MMP-2) in BBB disruptions and the upregulation of MMP-2 after chronic cerebral hypoperfusion in a rat model. In the present study, we asked whether MMP-2 is involved in the BBB disruption and the subsequent WM lesions after chronic cerebral hypoperfusion.

Methods—We compared the severity of white matter lesions in rats after chronic cerebral hypoperfusion with or without an MMP inhibitor. Then, we also induced the chronic cerebral hypoperfusion in wild-type and MMP-2-null mice.

Results—In the rats treated with a relatively selective MMP-2 inhibitor, AG3340, the WM lesions after chronic cerebral hypoperfusion were significantly less severe, and the number of activated astroglia and microglia were also significantly lower as compared with the vehicle-treated rats. Gene knockout of MMP-2 also reduced the severity of the WM lesions and the number of activated astroglia and microglia in a mice system. In both rodents, the disruption of BBB function, as assessed by IgM staining and the Evans blue extravasation test, was less severe when MMP-2 activity was attenuated.

Conclusions—These findings indicate that MMP-2 plays a critical role in the BBB disruption, glial cell activation, and WM lesions after chronic cerebral hypoperfusion and suggest the potential value of MMP-2 inhibitors as a therapeutic tool in cerebrovascular WM lesions. (***Stroke***. **2006;37:2816-2823.**)

Key Words: blood–brain barrier ■ chronic cerebral hypoperfusion ■ MMP inhibitor ■ MMP-2 ■ white matter lesion

Cerebrovascular white matter (WM) lesions, a neurodegenerative condition characterized by hyperintense signals on magnetic resonance images, are frequently associated with aging and cerebrovascular disease and are responsible for the cognitive decline of the elderly. Chronic cerebral ischemia is likely to cause these WM lesions, because cerebral blood flow is decreased in these patients.[1] Indeed, similar WM lesions can be induced in rats and mice after chronic cerebral hypoperfusion, the experimental conditions mimicking chronic cerebral ischemia in humans.[2,3]

Matrix metalloproteinases (MMPs) are a family of endopeptidases that can degrade most of the major constituents of the extracellular matrix.[4] MMP-2 and MMP-9 represent a subgroup of the MMP family and degrade several extracellular matrix components, including type IV collagen, fibronectin, and gelatin. Deregulated MMPs have been implicated in the tissue destruction associated with cancer, arthritis, and multiple sclerosis.[4] MMPs may also play a role in neurologic disorders. For instance, MMP-9 is increased in human brains after stroke,[5] and MMP-2 and MMP-3 are increased in cerebrovascular WM lesions from patients with vascular dementia.[6] A reduction in the basement membrane components, including type IV collagen, is associated with the blood–brain barrier (BBB) disruption during cerebral ischemia.[7] In our previous study on chronic cerebral hypoperfusion, the BBB disruption was accompanied by an upregulation of MMP-2 but not MMP-9,[8] suggesting the specific involvement of MMP-2 in the WM lesions. We hypothesize that the MMP-2 upregulation after chronic cerebral hypoperfusion correlates with BBB damage, which leads to glial activation and subsequent WM lesions. To clarify the cause–effect relationship among MMP-2 upregulation, BBB disruption, and WM lesions, we used 2 strategies to attenuate MMP-2 activity: an MMP inhibitor, AG3340, and MMP-2

Received March 2, 2006; final revision received June 9, 2006; accepted July 24, 2006.

From the Department of Neurology (K.N., M.I., R.T., H.T.), Horizontal Medical Research Organization (M.I.), the Department of Molecular Oncology (M.N.), and The 21st Century Center of Excellence Program, Department of Oncology (C.T.), Kyoto University Graduate School of Medicine, Kyoto, Japan; and the Laboratory for Behavioral Genetics (S.I.), RIKEN Brain Science Institute, Wako, Japan.

Correspondence to Kayoko Nakaji, MD, Department of Neurology, Graduate School of Medicine, Kyoto University, 54 Kawaharamachi, Shogoin, Sakyo-ku, Kyoto 606-8507, Japan. E-mail kann@kuhp.kyoto-u.ac.jp

Stroke **is available at http://www.strokeaha.org** **DOI: 10.1161/01.STR.0000244808.17972.55**

knockout. The results from both experiments strongly supported the idea that MMP-2 plays a critical role in BBB disruption and WM lesions.

Materials and Methods

Chronic Cerebral Hypoperfusion in Rats and Treatment With an Matrix Metalloproteinase Inhibitor

Chronic cerebral hypoperfusion with bilateral common carotid artery occlusion (BCAO) was induced in male Wistar rats (weight 150 to 200 g; Shimizu Experimental Supply; Kyoto, Japan) by double ligation of the common carotid arteries as previously described.[2] After the operation, the rats were kept in animal quarters with food and water ad libitum.

AG3340 (Agouron Pharmaceuticals) was dissolved at 75 mg/mL in 50% DMSO in propylenglycol. The rats were treated twice a day with an intraperitoneal injection of AG3340 (100 mg/kg) or vehicle (DMSO/propylenglycol) from just before the operation until 14 days after the operation. Similar doses and treatment paradigms have been shown to be effective in inhibiting MMP activity in gliomas in model animals.[9] Because our previous study demonstrated that the number of microglia peaked on 3 days and WM lesion started to become evident on 14 days after BCAO,[2] the animals were subjected to the analyses described subsequently.

Mice

The generation of C57BL/6J mice carrying the MMP-2-null allele has been described elsewhere.[10] In this mutant allele, a region containing the promoter and the first exon of the MMP-2 gene is replaced by the pgk-neo cassette. MMP-$2^{\pm}$ parents were mated to obtain both wild-type and MMP-$2^{-/-}$ (MMP-2-null) littermates. Genotyping was performed by polymerase chain reaction using the following primers: wild-type forward, CAACGATGGAGGCACGAGTG; wild-type reverse, GCCGGGGAACTTGATGATGG; mutant forward, CTTGGGTGGAGAGGCTATTC; and mutant reverse, AGGTGAGATGACAGGAGATC.

Chronic Cerebral Hypoperfusion in Mice and Cerebral Blood Flow Measurement

Adult male mice (weight 20 to 25 g) were subjected to bilateral common carotid arteries stenosis (BCAS) by applying the microcoils with an inner diameter of 0.18 mm to both common carotid arteries as previously described.[3] The cerebral blood flow (CBF) was recorded by laser Doppler flowmetry by placing a straight probe (OmegaFLO-N1; Neuroscience Inc) on 1 mm posterior and 2 mm lateral from bregma perpendicular to the skull bone through the guide cannula. The baseline CBF recordings were obtained just before and at 2 hours and 3, 7, 14, and 30 days after the surgery. The CBF values were expressed as a percentage of the baseline value.

Histochemical Evaluation of White Matter Lesions and Glial Activation

Under deep anesthesia, the animals were perfused with 10 mmol/L phosphate-buffered saline (300 mL for rats, 100 mL for mice) and then with a fixative consisting of 4% paraformaldehyde, 0.2% picric acid, and 0.1 mol/L phosphate buffer at pH 7.4 (300 mL for rats, 100 mL for mice). The brains were removed and postfixed for 24 hours in 4% paraformaldehyde in 0.1 mol/L phosphate buffer and then stored in 15% sucrose in 0.1 mol/L phosphate buffer. The fixed brains were embedded in paraffin and sliced into 2-μm-thick coronal sections. Klüver-Barrera staining and Bielschowsky staining were used to visualize the myelin sheaths and axons, respectively. As previously described,[2] the severity of the WM lesions was semiquantitatively graded as normal (grade 0), disarrangement of the nerve fibers (grade 1), formation of marked vacuoles (grade 2), and disappearance of myelinated fibers (grade 3) by an investigator blind to the experimental condition. For immunohistochemistry, serial sections (20-μm-thick) were cut in a cryostat and incubated overnight with a primary antibody at 4°C followed by incubation with the appropriate biotinylated secondary antibody (1 hour, room temperature), treatment with an avidin–biotin complex (diluted 1:200; Vector Laboratories), and visualization with 0.01% diaminobenzidine tetrahydrochloride and 0.005% H_2O_2 in 50 mmol/L Tris-HCl (pH 7.6). The primary antibodies used were as follows: monoclonal anti-rat glial fibrillary acidic protein (GFAP) (diluted 1:5000; Sigma-Aldrich; Mo, USA), polyclonal rabbit anti-mouse GFAP (diluted to 1:5000; Dako Cytomation, Denmark), polyclonal rabbit anti-MMP-2 (diluted to 1: 1,000, Chemicon International, Inc), monoclonal rat anti-mouse MHC class II antigen antibodies (diluted to 1:5000; Dako Cytomation), and rabbit anti Iba-1 antibody (1 μg/mL; Wako Pure Chemical Industries, Ltd; Osaka, Japan). Some sections were incubated with a biotinylated goat anti-rat IgM (μ), biotinylated goat anti-mouse IgM (μ) (diluted 1:1000; Kirkegaad & Perry Laboratories; Md, USA), or biotinylated Ricinus communis agglutinin-1 (diluted 1:1000; Vector Laboratories; Calif, USA) and were incubated directly with the avidin–biotin complex. To confirm the cellular source of IgM, sections were labeled by biotinylated anti-mouse IgM and rabbit anti-mouse GFAP followed by fluorescein isothiocyanate-labeled avidin (diluted 1:100; Dako Cytomation) and rhodamine-labeled goat anti- rabbit IgG (2.5 μL/mL; Dako). In the sections immunostained for Ricinus communis agglutinin-1, MHC class II antigen, Iba-1, GFAP, and IgM, we counted the number of immunopositive cells in at least 6 representative fields (per 0.25 mm^2) in the corpus callosum, the caudoputamen, and the optic tract for the quantitative analysis.

Zymography and Matrix Metalloproteinases-2 Activity Assay

Minced forebrain tissues were incubated with gentle rotation at 4°C for 20 hour in an extraction buffer consisting of 0.5% Triton-X 100, 0.5 U/mL aprotinin, and 0.01% sodium azide in 0.01 mol/L phosphate-buffered saline. The samples were then centrifuged at 14 000 rpm for 15 minutes at 4°C and the supernatants were collected. The protein content was adjusted to 10 mg/mL. The gelatinolytic activity of these samples was detected by SDS-PAGE zymography as described elsewhere,[8] although MMP-2 activity in the gray matter may interfere a sensitive detection of the activity in the WM. Equal amounts of tissue extract (50 μg) were then subjected to electrophoresis. To restore the activity of the protein, sample gels were agitated in 0.01 mol/L Tris-HCl (pH 8.0) containing 2.5% Triton X-100 (30 minutes×2). After washed in 0.05 mol/L Tris-HCl (pH 8.0) for 30 minutes, the gels were incubated overnight twice at 37°C in 0.05 mol/L Tris-HCl (pH 8.0) containing 0.5 mmol/L $CaCl_2$ and 1.0 mol/L $ZnCl_2$. After incubation, the gels were stained with Coomassie blue R-250. The amount of activated and latent forms of MMP-2 in the whole forebrain extracts were also assessed using the Matrix Metalloproteinase-2 Biotrak Activity Assay System (Amersham Biosciences), which is based on a 2-site enzyme-linked immunosorbent assay "sandwich" format and recognizes both the proform and active form of MMP-2.

Evans Blue Extravasation

The mice were killed at 3 hours and 1, 3, 5, 7, and 14 days after BCAS. One hour before each time point, 1 mL of 4% Evans blue (EB; Nakalai Chemicals Ltd) in normal saline was injected intraperitoneally. The animals were anesthetized and then perfused transcardially with 200 mL of 10 mmol/L phosphate-buffered saline. The brains were snap-frozen, sectioned into 20-μm-thick slices, and examined by fluorescence microscopy. For quantitative measures, the images were analyzed within 4 structurally similar areas (2 paramedian portions of the corpus callosum on each hemisphere) in each mouse and digitally level-adjusted by Adobe Photoshop (Adobe Systems) so that intravascular EB would be reported as white (pixel value 255) on a black background (pixel value 0). Using the public domain NIH Image 1.61 program (National Institutes of Health), the images were then binarized with intensity threshold set at pixel value 50 so that the white pixels represent intravascular and extravasated EB. The number of white pixels was divided by the total pixel

number in the selected area to estimate percent area containing intravascular and extravasated EB as an approximate index of BBB breakdown. Image analysis was focused on the paramedian portion of the corpus callosum facing the dorsal part of the lateral ventricle, because WM lesions were most intense in this region.[3]

Statistical Analysis

All data are presented as means±SE. A one-factor ANOVA followed by Fisher protected least significant difference procedure was used to compare the differences between groups. P values <0.05 were considered to be statistically significant.

Results

The amount of total MMP-2 in the forebrain extracts was comparable between the vehicle-treated and AG3340-injected rats after BCAO as assessed using the Biotrak Activity Assay System. The percentage of activated MMP-2 was only 7% on day 3 after the sham operation but was elevated to approximately 80% on day 3 after the BCAO (supplemental Figure I, available online at http://stroke.ahajournals.org). We also confirmed almost complete suppression of MMP-2 activation with AG3340 administration.

The operation was successful in rats (n=40) except 3, which developed convulsions and was killed within 7 days, and in mice (n=62) except 4, which developed cerebral infarction. These animals with unsuccessful operations were excluded from the statistical analysis. In the vehicle-treated animals, severe WM lesions, as shown by an increased number of disarranged nerve fibers and vacuolation, were found on day 14 after the BCAO in the optic nerve, medial part of the corpus callosum (Figure 1B and 1E), the internal capsule, and the fiber bundles of the caudoputamen. In such WM regions, the number of Ricinus communis agglutinin-1-positive microglia and GFAP-positive astroglia increased (2- to 3-fold) on day 3 after the BCAO (Figure 1H and 1K). Both WM lesions and gliosis were less severe in the AG3340-treated animals (Figure 1C, 1F, 1I, 1L, 1P through 1R, and Table 1).

The BBB integrity in rats subjected to BCAO was also assessed by the immunostaining for IgM. IgM-immunoreactive glial cells represent those cells that have taken up the serum proteins, which leaked into the brain parenchyma, and their number serves as an indicator of BBB dysfunction.[8] Some IgM-immunoreactive glial cells were found in the vicinity of the microvessels in the corpus callosum in the vehicle-treated animals on day 3 after the BCAO (Figure 1R), suggesting BBB dysfunction in this region. In contrast, much fewer IgM-immunoreactive glia were found in the same area of the AG3340-treated animals (Figure 1O and 1R).

These results strengthen the notion that MMPs play a role in BBB impairment and WM lesions. To further elucidate the roles of MMPs in the WM damage after chronic cerebral hypoperfusion, we applied BCAS (the established technique for mice hypoperfusion)[3] for mice lacking functional MMP-2 gene (MMP-2-null mice), which showed no obvious developmental abnormalities[10] or brain anomalies[11] and examined its effects using histochemical methods. The reduction of CBF after BCAS was comparable between wild-type and MMP-2-null mice. The CBF reductions (wild-type versus MMP-2-null; mean±SE %, n=3 each) were 42.5±4.3% versus 39.1±3.2% (2 hours after BCAS), 38.1±4.3 versus 39.4±4.0 (3 days), 35.2±4.6 versus 33.6±6.2 (7 days), 20.8±1.4 versus 26.9±3.1 (14 days), and 11.2±3.0 versus 24.0±4.0 (30 days). In wild-type mice, MMP-2-immunoreactive glial cells increased after BCAS compared with sham-operated mice (Figure 2A and 2B). MMP-9-immunoreactive cells were not induced after BCAS in both wild-type (Figure 2C and 2D) and MMP-2-null mice (Figure 2E). Consistently, zymography using forebrain homogenates revealed only a faint band of MMP-9 in the samples after BCAS for 3 days in both wild-type and MMP-2-null mice (n=4), whereas a robust band was found in the sample from a mouse with an incidental cerebral infarction after BCAS (Figure 2G). A band of MMP-2 was detected in the samples in wild-type mice but not in MMP-2-null mice after BCAS (n=4). However, zymography using such homogenates failed to show the upregulation of MMP-2 after 3 days of BCAS; regional upregulation of MMP-2 in the WM seemed obscured.

Klüver-Barrera staining revealed that WM lesions were predominant in the corpus callosum, caudoputamen, and internal capsule but not in optic tract on day 30 after BCAS in the wild-type mice. The medial part of the corpus callosum adjacent to the lateral ventricles was most severely affected (Figure 3E). In MMP-2-null mice, such WM lesions were far less severe (Figure 3I; Table 2). The mouse model showed little damage to the visual pathway and no difference was found between the wild-type mice and MMP-2-null mice after the operation. This may be attributable to the fact that BCAS in mice induces a milder decrease in the CBF than in the rat model and maintains a residual blood flow within the common carotid arteries and its branch, the ophthalmic artery.

In the wild-type mice on day 14 after BCAS, numerous activated microglia, as visualized by immunostaining with anti-MHC class II antibodies, were found in some WM regions (Figure 3F). In addition, the number of GFAP-immunoreactive astroglia increased in these mice (Figure 3G). In the MMP-2-null mice, the number of microglia and astroglia was much fewer in the WM as compared with the wild-type animals (Figure 3J, 3K, 3P, 3Q). Thus, both WM lesions and glial activation after chronic hypoperfusion were dramatically reduced in the MMP-2-null mice. There was no difference of the number of microglia, astroglia, and IgM-positive cells in optic tract (Figure 3P).

The BBB integrity in mice subjected to BCAS was assessed by the immunostaining for IgM and EB extravasation assay. After BCAS, the number of IgM-positive cells increased in the WM of the wild-type mice (Figure 3H) as compared with the sham-operated wild-type animals (Figure 3D). Intriguingly, the IgM-immunoreactive cells significantly decreased in the WM of MMP-2-null mice after BCAS (Figure 3L and 3R). IgM-immunoreactive cells were identified as astroglia based on their colabeling with GFAP in the perivascular areas (Figure 3L through 3O). Three days after BCAS, EB apparently leaked into the perivascular area in the corpus callosum (Figure 4B) and the cerebral cortex (data not shown). This extravasation was most notable in the paramedian portion of the corpus callosum. At all time points after BCAS, no extravasation of EB could be detected in the MMP-2-null mice (Figure 4C). The estimated percent area

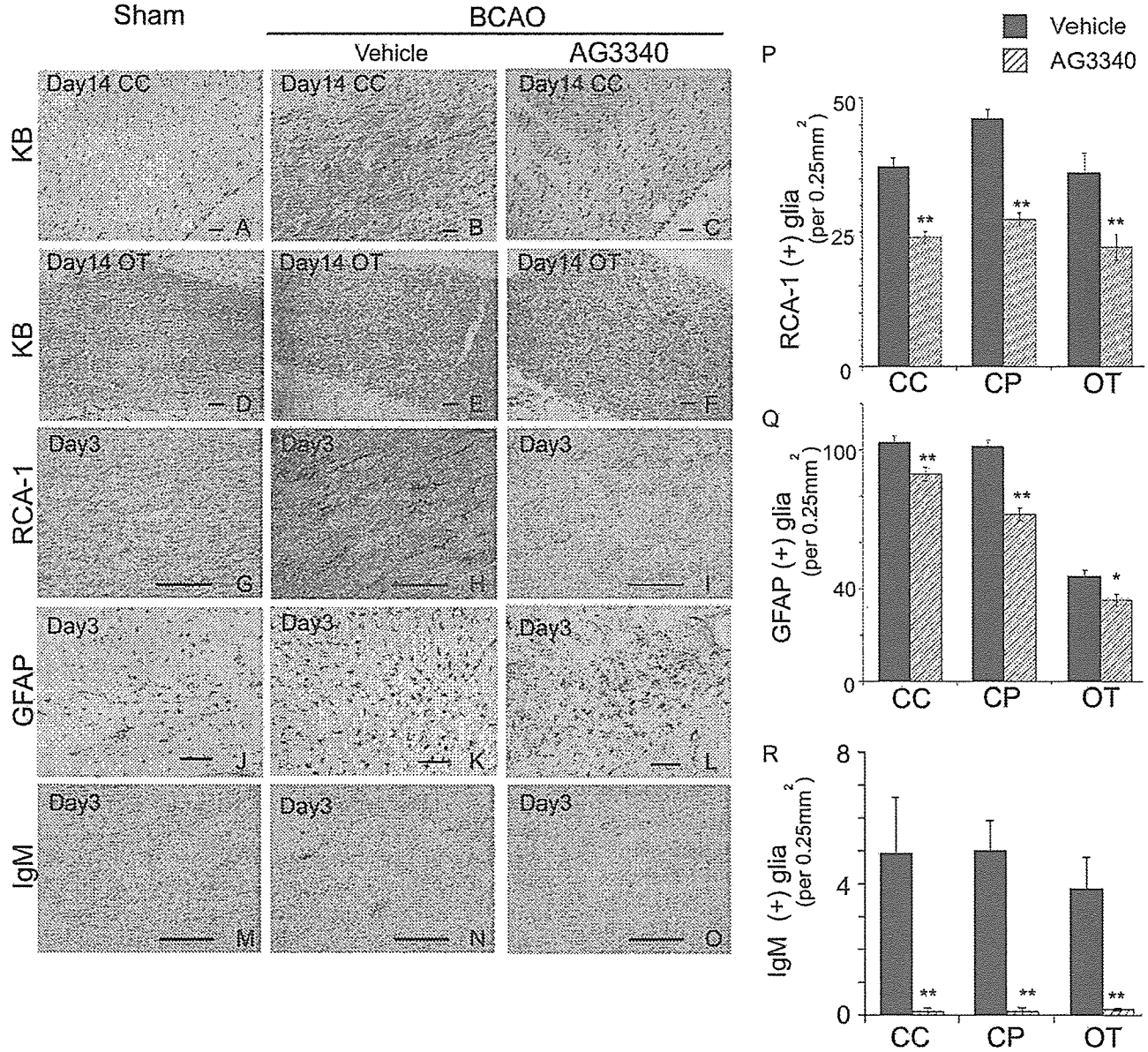

Figure 1. Histologic evaluation of the WM lesions in rats after chronic cerebral hypoperfusion with or without AG3340-treatment. A through O, Klüver-Barrera staining on day 14 (A through F; myelin sheath) or immunostaining on day 3 for Ricinus communis agglutinin-1 (G through I; microglia), GFAP (J through L; astroglia), or IgM (M through O) of the corpus callosum (A through C, G through O) and optic tract (D through F) of rats that had undergone sham operation (A, D, G, J, M) or BCAO operation, which had been treated either with vehicle (B, E, H, K, N) or AG3340 (C, F, I, L, O). Scale bar, 50 μm. (P through R) A histogram representing the density of cells immunoreactive for Ricinus communis agglutinin-1 (P), GFAP (Q), or IgM (R) in sections from the corpus callosum (CC), caudoputamen (CP), and optic tract (OT) in rats 3 days after a BCAO (n=4 each; *P<0.05, **P<0.01).

stained with EB was approximately 8% in wild-type mice after BCAS, which significantly reduced to 2% in MMP-2-null mice after BCAS (Figure 4D). Taken together, these results indicated that loss of MMP-2 alleviated BBB damage after BCAS and suggested a causative role for MMP-2 in the WM lesions after hypoperfusion.

TABLE 1. Histologic Grading of the WM Lesions in Untreated and AG3340-Treated Rats on Day 14 After BCAO

	Corpus Callosum	Caudoputamen	Optic Tract
Vehicle, N=5	1.3±045	1.4±0.54	2.6±0.55
AG3340, N=4	0.5±0.4*	0.63±0.25*	1.13±0.63*

*P<0.05.

Discussion

The synthetic MMP inhibitor AG3340 is known to inhibit several MMP family members, including MMP-2 (Ki=0.05 nmol/L), MMP-9 (0.26 nmol/L), MMP-13 (0.03 nmol/L), and MT1-MMP (0.33 nmol/L).[12] As a lipophilic, low-molecular-weight (Mr 423.5) compound, AG3340 can readily cross the BBB.[12] Using this compound, we have demonstrated that AG3340 shows protective effects against the WM lesions after chronic cerebral hypoperfusion in rats. This is consistent with our previous data using the same model, which showed a correlation of WM lesions with MMP-2 upregulation.[8] Then, AG3340 may have reduced the severity of WM lesions by inhibiting MMP-2 activation. In support of this notion,

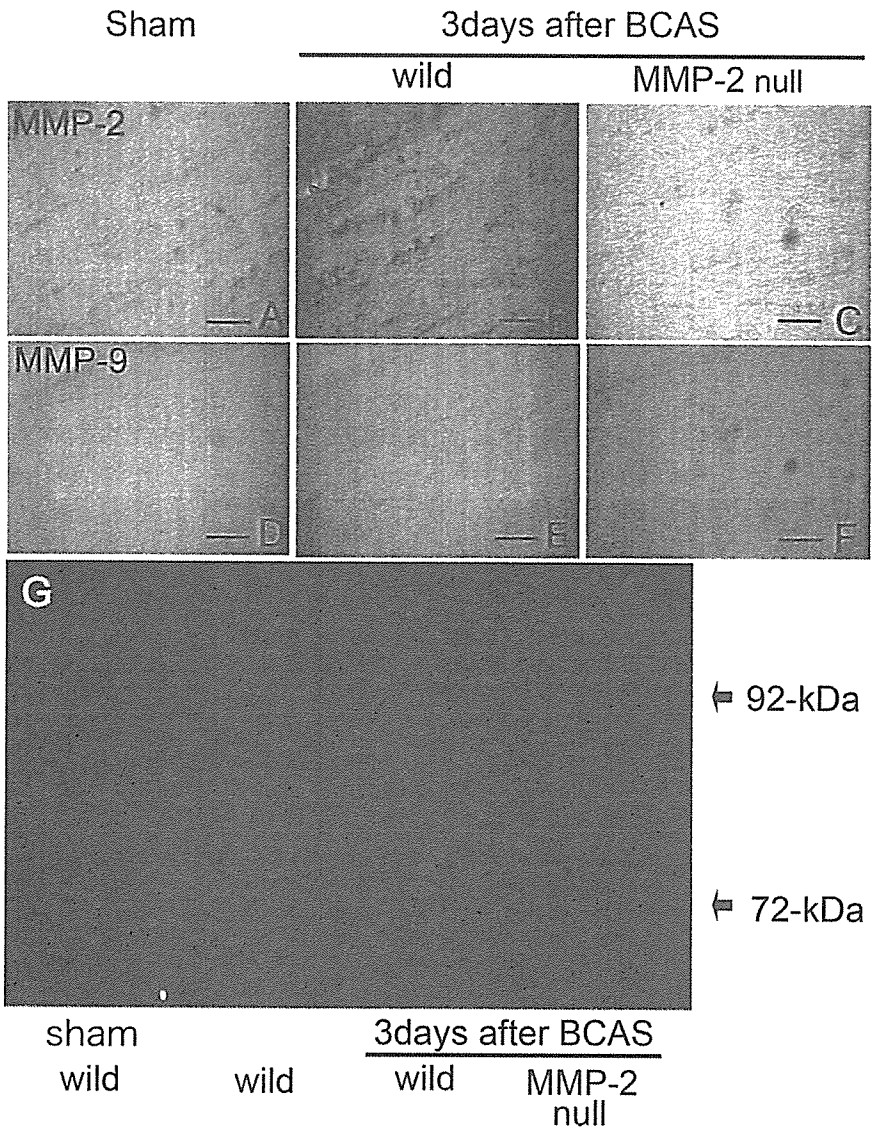

Figure 2. A through F, Immunohistochemical analysis for MMP-2 (A through C) and MMP-9 (D through F) in the corpus callosum of wild-type mice (A, B, D, E) or MMP-2-null mice (C, F) on day 3 after sham operation or BCAS (B, D). G, Zymography assay of the samples from a mouse with incidental cerebral infarction (CI), a wild-type mouse and an MMP-2-null mouse 3 days after BCAS. Note the absence of compensatory upregulation of MMP-9 in MMP-2-null mice.

genetic deletion of MMP-2 attenuated the WM lesions after chronic cerebral hypoperfusion in mice. These data jointly suggest that MMP-2 upregulation plays a major role in the WM lesions.

Previous studies have established the importance of the upregulation and activation of MMPs in acute brain ischemia.[13–15] Among the members of the MMP family (n≥20), MMP-9 is of particular interest in the context of acute brain ischemia, because the selective upregulation of MMP-9 has been observed in the brains of patients with stroke.[15] More importantly, the neuronal damage after cerebral ischemia was attenuated in the MMP-9-null mice compared with the wild-type mice.[16] Furthermore, Heo et al demonstrated association of MMP-9 upregulation with hemorrhagic transformation in the nonhuman primates.[17] Thus, MMP-9 upregulation may contribute to the BBB damage and infarct size, especially in the acute setting. Although previous study demonstrated the upregulation of MMP-9 in MMP-2-null mice,[18] no upregulation of MMP-9 was observed in our model, which suggested a negligible role of MMP-9 in chronic cerebral hypoperfusion.

What then would be the role of MMPs in cerebral ischemia? Hamann et al reported disappearance of the basal lamina around the microvessels during cerebral ischemia and reperfusion.[7] Fukuda et al demonstrated that the ischemic primate brain contained elevated levels of activity enough to digest basal lamina components such as type IV collagen.[19] In fact, Heo et al indicated that MMP-2 upregulated significantly by 1 hour after MCAO[18] and was persistently elevated thereafter in primates, and Chan et al demonstrated the upregulation of activation system for latent MMP-2 after focal cerebral ischemia.[20] These findings support the hypothesis that excessive degradation of the vascular basal lamina is a mechanism by which MMP triggers BBB dysfunction, edema, hemorrhage. The most marked extravasation of Evans blue in the paramedian portion of the corpus callosum facing the lateral ventricle was consistent with a previous report on a rat model of chronic cerebral hypoperfusion[21] and further indicated a vulnerability of the BBB in this area. In the case of chronic hypoperfusion, a previous study suggested the association of MMP-2 but not MMP-9 upregulation with BBB disruption. Consistently, Rosenberg et al showed that the activated

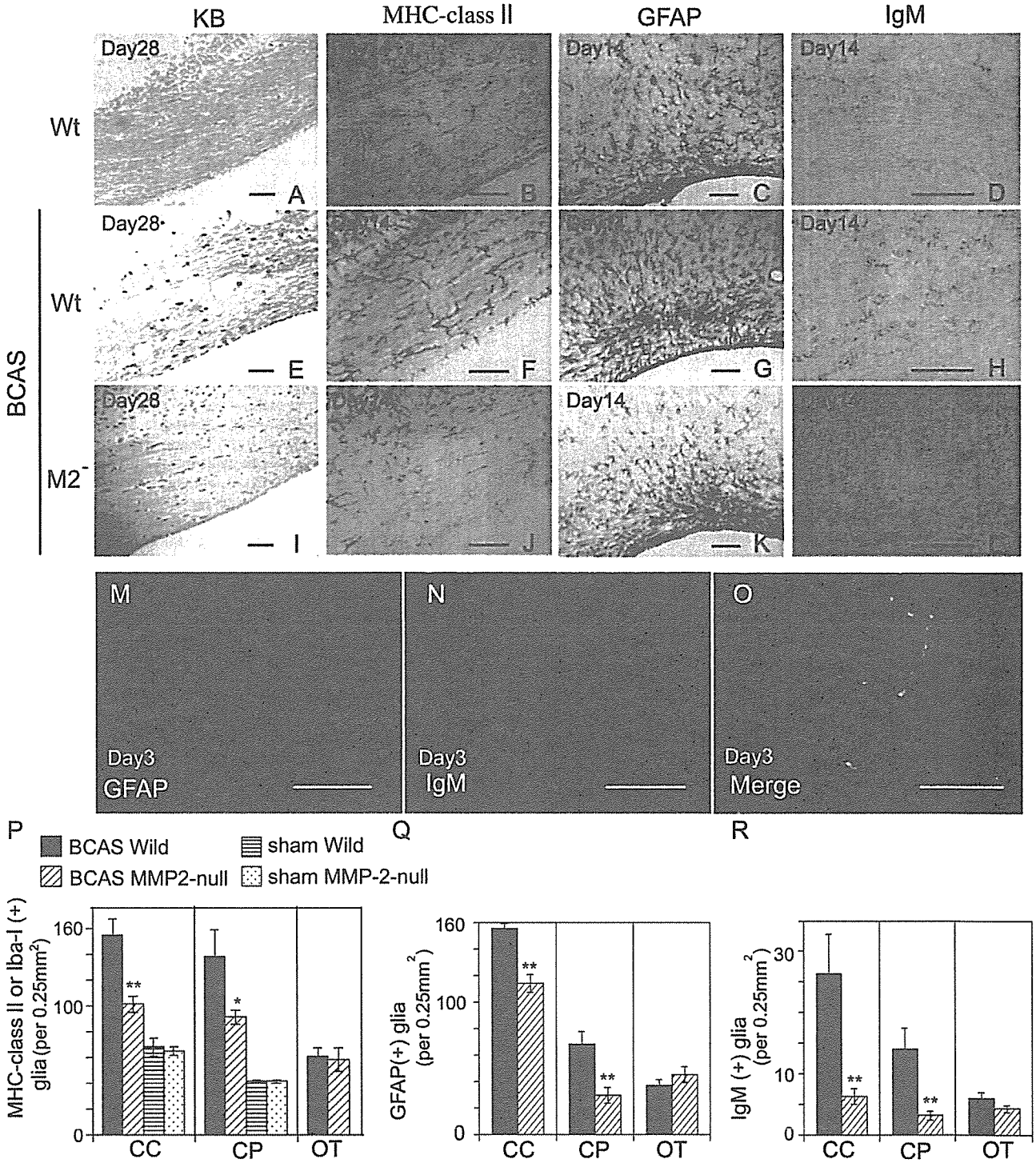

Figure 3. Histologic evaluation of the WM lesions in wild-type and MMP-2-null mice after BCAS. A through L, Klüver-Barrera staining 28 days after BCAS (A, E, I) and immunostaining 14 days after BCAS for MHC class II (B, F, J), GFAP (C, G, K), or IgM (D, H, L) of corpus callosum sections from wild-type (Wt) mice (A through H) or MMP-2-null (M2$^-$) mice (I through L) that had undergone either a sham operation (A through D) or BCAS (E through L). Note that MMP-2 gene knockout recover the decrease of Klüver-Barrera staining in the WM after BCAS (compare E with I) and glial activation (compare F with J for microglia and G with K for astroglia). Scale bar, 50 μm. M through O, Double staining with GFAP and IgM of the WM lesions in wild-type mice after BCAS. IgM was observed on endfeet of GFAP-positive glia (O). Scale bar, 10 μm. P through R, A histogram representing the density of cells immunoreactive for MHC-class II or Iba-I (P), GFAP (Q), or IgM (R) in sections from the corpus callosum (CC), caudoputamen (CP), and optic tract (OT) of mice that had undergone BCAS (n=6 each; *P<0.05, **P<0.01). For the microglial count, anti-MHC-class II antibodies were used for mice with BCAS operation, whereas anti-Iba-I antibodies were used for mice with sham operation (P). Note that glial activation was not observed in the optic tract, being consistent with the absence of rarefaction of this structure.

TABLE 2. Histologic Grading of the WM Lesions in Wild-Type and MMP-2-Null Mice on Day 30 After BCAS

	Corpus Callosum	Caudoputamen	Anterior Commissure
Wild-type, N=6	1.5±0.8	1.3±0.58	0.5±0.5
MMP-2-null, N=6	0.5±0.8*	0.58±0.37*	0±0

*$P<0.05$.

astroglia and microglia/macrophages around the arterioles expressed MMP-2 and MMP-3, but not MMP-9, in the brains of patients with vascular dementia.[6]

Caplan[22] proposed that the major pathologic features of WM lesions such as demyelination and gliosis may result from a BBB dysfunction, which allows the leakage of proteins and fluid through the compromised barrier of the penetrating arteries. This hypothetical pathway is consistent with our present findings. Given the overlapping substrate specificity between MMP-2 and MMP-9, in the case of chronic cerebral hypoperfusion, MMP-2 may contribute to the BBB disruption through the excessive digestion of the vascular basal lamina and activation of glia. In addition, MMP-2 may be directly involved in demyelination associated with WM lesions, because MMP-2 can digest myelin more efficiently than MMP-9.[24]

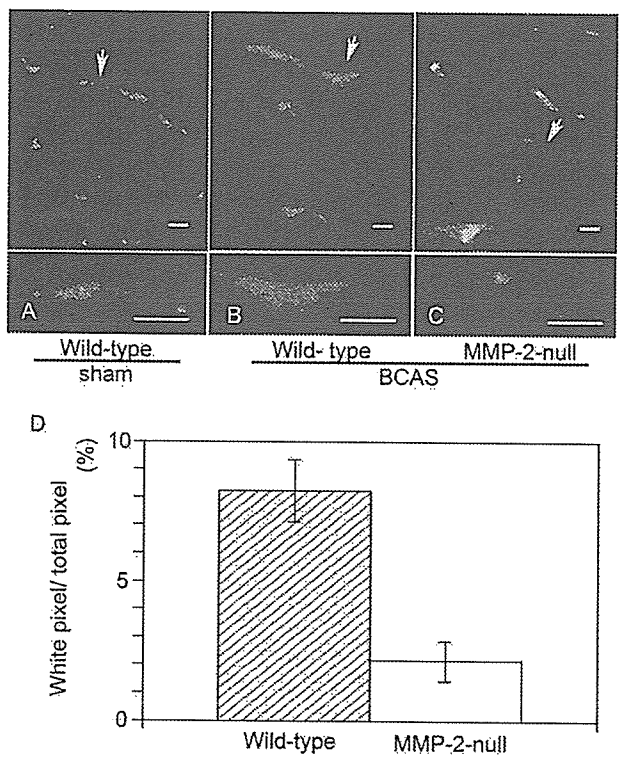

Figure 4. Evaluation of BBB dysfunction in the corpus callosum of mice. The Evans blue extravasation assay was performed on day 3 after a sham operation in wild-type mice (A) or on day 3 after BCAS in wild-type (B) and MMP-2-null mice (C). A magnified view of the area indicated by an arrow in the upper panel is shown in the lower panel (A through C). The experiments were repeated in triplicate with similar findings (n=4 each). Scale bar, 100 μm. A histogram representing the degree of Evans blue extravasation as an approximate index of BBB breakdown (see "Methods") (D).

In conclusion, the present study has provided direct evidence that MMP-2 is involved in the pathogenesis of WM lesions in the mouse model. Although the species difference between rodents and humans should be taken into consideration, our data also suggest the potential value of MMP inhibitors in preventing subcortical ischemic vascular dementia resulting from BBB dysfunction and chronic cerebral ischemia in humans. Activation of MMP-2 is reported to participate in matrix injury during focal cerebral ischemia. An elucidation of the exact roles of MMP-2 in BBB disruption may also provide information useful in developing strategies for controlling neuroinflammation in general.

Acknowledgments

The authors are indebted to Miss Nakabayashi for her excellent technical assistance.

Disclosures

None.

References

1. Meguro K, Hatazawa J, Yamaguchi T, Itoh M, Matsuzawa T, Ono S, Miyazawa H, Hishinuma T, Yanai K, Sekita Y. Cerebral circulation and oxygen metabolism associated with subcortical perivascular hyperintensity as shown by magnetic resonance imaging. *Ann Neurol.* 1990;28:378–383.
2. Wakita H, Tomimoto H, Akiguchi I, Kimura J. Glial activation and white, matter changes in the rat brain induced by chronic cerebral hypoperfusion: an immunohistochemical study. *Acta Neuropathol.* 1994;87:484–492.
3. Shibata M, Ohtani R, Ihara M, Tomimoto H. White matter lesions and glial activation in a novel mouse model of chronic cerebral hypoperfusion. *Stroke.* 2004;35:2598–2603.
4. Sternlicht MD, Werb Z. How matric metalloproteinases regulate cell behavior. *Annu Rev Cell Dev Biol.* 2001;17:463–516.
5. Clark AW, Krekoski CA, Bou SS, Chapman KR, Edwards DR. Increased gelatinase A (MMP-2) and gelatinase B (MMP-9) activities in human brain after focal ischemia. *Neurosci Lett.* 1997;238:53–56.
6. Rosenberg GA, Sullivan N, Esiri MM. White matter damage is associated with matrix metalloproteinases in vascular dementia. *Stroke.* 2001;32:1162–1168.
7. Hamann GF, Okada Y, Fitridge R, del Zoppo GJ. Microvascular basal lamina antigens disappear during cerebral ischemia and reperfusion. *Stroke.* 1995;26:2120–2126.
8. Ihara M, Tomimoto H, Kinoshita M, Oh J, Noda M, Wakita H, Akiguchi I, Shibasaki H. Chronic cerebral hypoperfusion induces MMP-2 but not MMP-9 expression in the microglia and vascular endothelium of the white matter. *J Cereb Blood Flow Metab.* 2001;21:828–834.
9. Price A, Shi Q, Morris D, Wilcox ME, Brasher PM, Rewcastle NB, Shalinsky D, Zou H, Appelt K, Johnston RN, Yong VW, Edwards D, Forsyth P. Marked inhibition of tumor growth in a malignant glioma tumor model by a novel synthetic matrix metalloproteinase inhibitor AG3340. *Clin Cancer Res.* 1999;4:845–854.
10. Itoh T, Ikeda T, Gomi H, Nakao S, Suzuki T, Itohara S. Unaltered secretion of beta-amyloid precursor protein in gelatinase A (matrix metalloproteinase 2)-deficient mice. *J Biol Chem.* 1997;272:22389–22392.
11. Asahi M, Sumii T, Fini ME, Itohara S, Lo EH. Matrix metalloproteinase 2 gene knockout has no effect on acute brain injury after focal ischemia. *Neuroreport.* 2001;12:3003–3007.
12. Shalinsky DR, Brekken J, Zou H, McDermott CD, Forsyth P, Edwards D, Margosiak S, Bender S, Truitt G, Wood A, Varki NM, Appelt K. Broad antitumor and antiangiogenic activities of AG3340, a potent and selective MMP inhibitor undergoing advanced oncology clinical trials. *Ann N Y Acad Sci.* 1999;878:236–270.
13. Rosenberg GA, Navratil M, Barone F, Feuerstein G. Proteolytic cascade enzymes increase in focal cerebral ischemia in rat. *J Cereb Blood Flow Metab.* 1996;16:360–366.

14. Horstmann S, Kalb P, Koziol J, Gardner H, Wagner S. Profiles of matrix metalloproteinases, their inhibitors, and laminin in stroke patients: influence of different therapies. *Stroke*. 2003;34:2165–2170.
15. Maier CM, Hsieh L, Yu F, Bracci P, Chan PH. Matrix metalloproteinase-9 and myeloperoxidase expression: quantitative analysis by antigen immunohistochemistry in a model of transient focal cerebral ischemia. *Stroke*. 2004; 5:1169–1174.
16. Lee SR, Tsuji K, Lee SR, Lo EH. Role of matrix metalloproteinase in delayed neuronal damage after transient global ischemia. *J Neurosci*. 2004;24:671–678.
17. Heo JH, Lucero J, Abumiya T, Koziol JA, Copeland BR, del Zoppo GJ. Matrix metalloproteinases increase very early during experimental focal cerebral ischemia. *J Cereb Blood Flow Metab*. 1999;19:624–633.
18. Esparza J, Kruse M, Lee J, Michaud M, Madri JA. MMP-2 null mice exhibit an early onset and severe experimental autoimmune encephalomyelitis due to an increase in MMP-9 expression and activity. *FASEB J*. 2004;18:1682–1691.
19. Fukuda S, Fini CA, Mabuchi T, Koziol JA, Eggleston LL Jr, del Zoppo GJ. Focal cerebral ischemia induces active proteases that degrade microvascular matrix. *Stroke*. 2004;35:998–1004.
20. Chang DI, Hosomi N, Lucero J, Heo JH, Abumiya T, Mazar AP. Activation system for latent matrix metalloproteinase-2 are upregulated immediately after focal cerebral ischemia. *J Cereb Blood Flow Metab*. 2003;23:1408–1419.
21. Ueno M, Tomimoto H, Akiguchi I, Wakita H, Sakamoto H. Blood–brain barrier disruption in white matter lesions in a rat model of chronic cerebral hypoperfusion. *J Cereb Blood Flow Metab*. 2002; 22:97–104.
22. Caplan LR. Dilatative arteriopathy (dolichoectasia): what is known and not known. *Ann Neurol*. 2005;57:472–479.
23. Chandler S, Coates R, Gearing A, Lury J, Wells G, Bone E. Matrix metalloproteinases degrade myelin basic protein. *Neurosci Lett*. 1995; 201:223–226.

Journal of Neurochemistry, 2006, **99**, 1456–1469 doi:10.1111/j.1471-4159.2006.04155.x

A ubiquitin ligase HRD1 promotes the degradation of Pael receptor, a substrate of Parkin

Tomohiro Omura,*,** Masayuki Kaneko,*,** Yasunobu Okuma,*,** Yasuko Orba,† Kazuo Nagashima,† Ryosuke Takahashi,†† Noboru Fujitani,‡ Satoshi Matsumura,‡ Akihisa Hata,‡ Kyoko Kubota,* Karin Murahashi,* Takashi Uehara* and Yasuyuki Nomura*,¶,§

**Department of Pharmacology, Graduate School of Pharmaceutical Sciences, Hokkaido University, Sapporo, Japan*

***Department of Pharmacology, Faculty of Pharmaceutical Sciences, Chiba Institute of Science, Choshi, Chiba, Japan*

†Laboratory of Molecular and Cellular Pathology, Hokkaido University Graduate School of Medicine, Sapporo, Japan

††Department of Neurology, Kyoto University Graduate School of Medicine, Kyoto, Japan

‡Division of Clinical Laboratory Science, Department of Environmental Security System, Faculty of Risk and Crisis Management, Chiba Institute of Science, Choshi, Chiba, Japan

¶Hokkaido University Graduate School of Medicine, Sapporo, Japan

§Yokohama College of Pharmacy, Yokohama, Japan

Abstract

It has been proposed that in autosomal recessive juvenile parkinsonism (AR-JP), a ubiquitin ligase (E3) Parkin, which is involved in endoplasmic reticulum-associated degradation (ERAD), lacks E3 activity. The resulting accumulation of Parkin-associated endothelin receptor-like receptor (Pael-R), a substrate of Parkin, leads to endoplasmic reticulum stress, causing neuronal death. We previously reported that human E3 HRD1 in the endoplasmic reticulum protects against endoplasmic reticulum stress-induced apoptosis. This study shows that HRD1 was expressed in substantia nigra pars compacta (SNC) dopaminergic neurons and interacted with Pael-R through the HRD1 proline-rich region, promoting the ubiquitylation and degradation of Pael-R. Furthermore, the disruption of endogenous HRD1 by small interfering RNA (siRNA) induced Pael-R accumulation and caspase-3 activation. We also found that ATF6 overexpression, which induced HRD1, accelerated and caused Pael-R degradation; the suppression of HRD1 expression by siRNA partially prevents this degradation. These results suggest that in addition to Parkin, HRD1 is also involved in the degradation of Pael-R.

Keywords: endoplasmic reticulum stress; endoplasmic reticulum-associated degradation; HRD1; Parkin-associated endothelin receptor-like receptor; Parkinson's disease; unfolded protein response

J. Neurochem. (2006) **99**, 1456–1469.

Parkinson's disease is the most common movement disorder and the second most common neurodegenerative disease. Only approximately 5% of Parkinson's disease patients are familial. Autosomal recessive juvenile parkinsonism (AR-JP) occurs with increasing frequency in familial Parkinson's disease patients and results from parkin gene (*PARK2*) mutations (Kitada *et al.* 1998). In AR-JP patients, the loss of dopaminergic neurons and the appearance of parkinsonism symptoms occur without the formation of Lewy bodies,

Received June 13, 2006; revised manuscript received July 21, 2006; accepted July 21, 2006.

Address correspondence and reprint requests to Yasuyuki Nomura, Yokohama College of Pharmacy, Yokohama 245–0066, Japan.
E-mail: nomura@pharm.hokudai.ac.jp

Abbreviations used: AR-JP, autosomal recessive juvenile parkinsonism; DAB, diaminobenzidine; DMEM, Dulbecco's modified Eagle's medium; DTT, dithiothreitol; ERAD, endoplasmic reticulum-associated degradation; E3, ubiquitin ligase; E2, ubiquitin-conjugating enzyme; FCS, fetal calf serum; GFAP, glial fibrillary acidic protein; GFP, green fluorescent protein; IPTG, isopropyl-β-D-thiogalactopyranoside; Pael-R, Parkin-associated endothelin receptor-like receptor; PBS, phosphate-buffered saline; PMSF, phenylmethylsulfonyl fluoride; HRD, HMG-CoA reductase degradation; SEL, suppressor or enhancer of lin-12; SDS-PAGE, sodium dodecyl sulfate–polyacrylamide gel electrophoresis; SNC, substantia nigra pars compacta; UPR, unfolded protein response; XBP1, X-box binding protein 1; ATF6, activating transcription factor 6; UPS, ubiquitin-proteasome system.

which are a significant characteristic of non-familial and some familial Parkinson's disease cases (Mizuno *et al.* 1998).

Eukaryotic cells coordinate the folding and glycosylation of secretary and membrane proteins in the endoplasmic reticulum. Various stresses leading to impairment of the endoplasmic reticulum and the production of mutant proteins cause the accumulation of unfolded proteins in the endoplasmic reticulum, culminating in cell death. Unfolded proteins accumulated in the endoplasmic reticulum are degraded by the ubiquitin-proteasome system (UPS). In this endoplasmic reticulum system, termed endoplasmic reticulum-associated degradation (ERAD), unfolded proteins are initially retrotranslocated from the endoplasmic reticulum to the cytosol through the translocon, polyubiquitylated by ubiquitin-conjugating enzyme (E2), ubiquitin ligase (E3), and other components, and degraded by the 26S proteasome (Hershko and Ciechanover 1998). E3 plays an important role in the ubiquitylation of unfolded proteins, and the RING finger domain of E3 mediates the transfer of ubiquitin from E2 to substrates (Zheng *et al.* 2000).

Parkin is an E3 that contains two RING finger domains; AR-JP-linked Parkin mutants have defective E3 activity. Parkin is up-regulated in response to endoplasmic reticulum stress and protects against cell death caused by such stress, suggesting that it is an E3 involved in ERAD. Parkin-associated endothelin receptor-like receptor (Pael-R) has been identified as a protein that interacts with Parkin; its accumulation leads to endoplasmic reticulum stress-induced cell death. Parkin ubiquitinates and promotes the degradation of insoluble Pael-R, resulting in the suppression of cell death (Imai *et al.* 2001). In other words, endoplasmic reticulum stress caused by the accumulation of unfolded Pael-R might be involved in AR-JP. Furthermore, it has been recently reported that Pael-R in Parkinson's disease is accumulated in the core of Lewy bodies (Murakami *et al.* 2004) and that selective dopaminergic neurodegeneration is caused by the ectopic expression of human Pael-R in the *Drosophila* brain (Yang *et al.* 2003).

It is known that in yeast, Hrd1p/Der3p is involved in ERAD. Hrd1p/Der3p is localized in the endoplasmic reticulum, contains the RING-finger domain at the C-terminus, and ubiquitinates substrates including HMG-CoA reductase (Hmg2p) (Gardner *et al.* 2000, 2001; Deak and Wolf 2001). Hrd3p is reported to regulate or stabilize Hrd1p (Plemper *et al.* 1999; Deak and Wolf 2001). Endoplasmic reticulum stress induces various components involved in ERAD, including Hrd1p as well as endoplasmic reticulum molecular chaperones, suggesting that ERAD involves the degradation of unfolded proteins in cooperation with endoplasmic reticulum chaperones (Friedlander *et al.* 2000; Travers *et al.* 2000). We previously reported that human HRD1 was identified and characterized as a human homolog of yeast Hrd1p (Kaneko *et al.* 2002). In that report, we demonstrated that HRD1 possesses E3 activity, is induced during endoplasmic reticulum stress, and suppresses cell death caused by endoplasmic reticulum stress. Furthermore, human HRD1 is reportedly involved in the basal, and not the sterol-regulated, degradation of HMG-CoA reductase (Nadav *et al.* 2003; Kikkert *et al.* 2004) and is a pathogenic factor in rheumatoid arthritis (Amano *et al.* 2003).

The unfolded protein response (UPR) is required for the inhibition of further protein synthesis and the induction of endoplasmic reticulum chaperones, which reduce the number of unfolded proteins in the endoplasmic reticulum (Kaufman 1999, 2002). Transcription factor ATF6 is a transmembrane protein localized in the endoplasmic reticulum (Haze *et al.* 1999). Under endoplasmic reticulum stress, ATF6 is cleaved to release the N-terminal fragment on the cytosolic side of the membrane; it then enters the nucleus, acts as a transcription factor, and eventually activates endoplasmic reticulum chaperone gene transcription, which enhances protein folding (Haze *et al.* 1999; Ye *et al.* 2000; Shen *et al.* 2002). On the other hand, an endoplasmic reticulum-resident transmembrane protein IRE1, which possesses serine/threonine kinase and RNase domains, is dimerized and autophosphorylated during endoplasmic reticulum stress (Cox *et al.* 1993; Sidrauski and Walter 1997). Activated IRE1 splices XBP1 mRNA and then generates an active form of XBP1 (Yoshida *et al.* 2001).

Recent studies have demonstrated that Parkin knockout mice exhibit no significant change in either dopaminergic neurodegeneration or the accumulation of any Parkin substrates (Goldberg *et al.* 2003; Itier *et al.* 2003; Palacino *et al.* 2004; Von Coelln *et al.* 2004; Perez and Palmiter 2005; Periquet *et al.* 2005), suggesting that other unknown E3s can degrade accumulated proteins in the absence of Parkin. On the other hand, HRD1 apparently degrades a number of unfolded proteins as overexpressed HRD1 protects against endoplasmic reticulum stress-induced cell death. This study showed that human HRD1 was located in substantia nigra pars compacta (SNC) neurons in the mouse brain. Therefore, we hypothesized that HRD1 as well as Parkin ubiquitinates and degrades the unfolded Pael-R responsible for endoplasmic reticulum stress and protects against Pael-R-induced cell death. In addition, we investigated whether ATF6-induced UPR activation promotes the degradation of Pael-R and whether UPR-induced HRD1 expression is partially involved in this degradation.

Materials and methods

Constructs

The expression vector for human wild-type and truncated fragments of HRD1 was tagged with myc and polyhistidine (6 × His) epitopes at the C-terminus of the inserted sequence (pcDNA6; Invitrogen Corporation, Carlsbad, CA, USA). Human Pael-R (pcDNA3),

tagged with FLAG and 6 × His epitopes at the C-terminus, was a gift from Ryosuke Takahashi (RIKEN Brain Science Institute, Japan). The expression vector for wild-type human α-synuclein, tagged with hemagglutinin and 6 × His epitopes at the C-terminus, was cloned into expression vector pcDNA3.1 (Invitrogen). The expression vector for the cleaved form of ATF6 (amino acid region 1–373 of ATF6α), tagged with hemagglutinin epitopes at the N-terminus was cloned into expression vector pCR3.1 (Invitrogen). The expression vector for RP-HRD1 fused at its N-terminus to glutathione S-transferase (GST) was cloned into the expression vector pGEX6p-1 (GE Healthcare Bio-Sciences, Piscataway, NJ, USA).

Affinity-purified antibodies, chemicals, and proteins

HRD1 polyclonal antibody against the KLH-conjugated synthetic peptide (C)-EDGEPDAAELRRR, corresponding to amino acid residues 594–606 of human HRD1 protein, was recognized human and mouse HRD1 (a gift from Otsuka GEN Research Institute). We also purchased anti-HRD1 polyclonal antibody (C-term) from Abgent (San Diego, CA, USA). Anti-Pael-R polyclonal antibody was used as described (Imai *et al.* 2001). Anti-FLAG M2 polyclonal and HRP-conjugated M2 monoclonal antibodies, and M2 affinity gel were purchased from Sigma-Aldrich (St. Louis, MO, USA); anti-calreticulin polyclonal and anti-KDEL monoclonal antibodies were from Stressgen Biotechnologies Corporation (Ann Arbor, MI, USA); anti-myc monoclonal (9E10) antibody was from Oncogene Research Products (Cambridge, MA, USA); anti-caspase-3 (Asp175) polyclonal antibody was from Cell Signaling Technology Inc. (Danvers, MA, USA); anti-GST polyclonal (Z-5) and anti-hemagglutinin polyclonal (Y-11) antibodies were from Santa Cruz Biotechnology (Santa Cruz, CA, USA); MG132 was from the Peptide Institute (Osaka, Japan), and rabbit ubiquitin-activating enzyme (E1), GST-UbcH5c (E2), and GST-ubiquitin were from BostonBiochem (Cambridge, MA, USA). Horseradish peroxidase-conjugated anti-mouse IgG and anti-rabbit IgG (both from GE Healthcare Bio-sciences) were used as the secondary antibody. Bands were detected using the enhanced chemiluminescence (ECL) system (GE Healthcare Bio-Sciences).

Immunohistochemistry

Mouse brains were fixed in 4% paraformaldehyde, processed on a Tissue-Tek VIP (Sakura Finetek, Tokyo, Japan), and then embedded in paraffin. The brains were sectioned into 4-μm-thick slices, mounted on silane-coated slides, and then subjected to heat treatment with 10 mM sodium citrate buffer (pH 6.0) in a pressure cooker for 3 min. Diaminobenzidine (DAB) immunostaining was performed using anti-HRD1 polyclonal antibody as the primary antibody (1 : 50 dilution), a peroxidase-labeled polymer-conjugated anti-rabbit antibody (Envision system; Dako, Glostrup, Denmark), and DAB as the substrate.

Immunofluorescence staining was stained with anti-HRD1 polyclonal antibody (1 : 20 dilution) and either anti-neuron-specific nuclear protein (NeuN; 1 : 100 dilution; Chemicon International, Temecula, CA, USA), anti-glial fibrillary acidic protein (GFAP; 1 : 100 dilution; Chemicon International), or anti-tyrosine hydroxylase (1 : 100 dilution; Chemicon International) monoclonal antibodies, and then with anti-mouse antibody conjugated with Alexa 546 and anti-rabbit antibody with Alexa 488 (Molecular Probes, Eugene, OR, USA). Fluorescence images were acquired using a Zeiss LSM 510 confocal microscope (Carl Zeiss AG, Gottingen, Germany).

Immunocytochemistry

For the subcellular localization of HRD1 and Pael-R, COS-1 cells were transfected with HRD1-myc or a control vector (Mock) and Pael-R-FLAG using the calcium phosphate method. To visualize the effect of HRD1 degrading Pael-R, normal human embryonic kidney (HEK293) cells and those stably transfected with HRD1-myc and M-HRD1-myc were transfected with Pael-R-FLAG-pcDNA3 and DsRED-express-N1 vector (Promega, Madison, WI, USA) using LipofectAMINE 2000 (Invitrogen). At 36 h after transfection, the cells were fixed with methanol at −20°C. The cells were then stained for the presence of proteins with appropriate primary antibodies, and then with anti-mouse antibody conjugated with Alexa 488 and/or anti-rabbit antibody with Alexa 594 (Molecular Probes). Fluorescence images were acquired using a Zeiss LSM 510 confocal microscope (Carl Zeiss AG, Gottingen, Germany).

Immunoprecipitation and western blotting

Transfected HEK293 cells were lysed in a lysis buffer [20 mM HEPES (pH 7.4), 120 mM NaCl, 5 mM EDTA, 10% glycerol, and 1% Triton X-100 with complete protease inhibitors (Roche Diagnostics K.K., Basel, Switzerland)]. Immunoprecipitation was carried out by incubating the supernatant with the indicated antibodies for 16 h and then with Protein G Sepharose Fast Flow (GE Healthcare Bio-sciences) for 1 h. For immunoprecipitation with an anti-FLAG antibody, the supernatant was incubated with anti-FLAG M2 affinity gel for 16 h. The immune complex was rinsed with a washing buffer [10 mM Tris-HCl (pH 7.5), 100 mM NaCl, 10% glycerol, and 0.2% Triton X-100].

Pulse-chase experiment

Neuro2a cells were transfected with Pael-R-FLAG and either a control vector, HRD1-myc or M-HRD1-myc. At 36 h after transfection, the cells were starved for 1 h in methionine/cysteine-free Dulbecco's modified Eagle's medium (DMEM; Sigma) containing 5% dialyzed fetal calf serum (FCS), and then labeled for 1 h at 37°C with 100 μCi/mL [^{35}S]-methionine/cysteine (Redivue Promix L-[^{35}S] *in vitro* cell labeling mix; GE Healthcare Bio-Sciences). The cells were then washed and incubated in DMEM containing 10% FCS for the indicated periods. The cell lysates were immunoprecipitated with the anti-FLAG antibody, subjected to sodium dodecyl sulfate–polyacrylamide gel electrophoresis (SDS-PAGE), and visualized using an imaging analyzer (BAS-2500, Fujifilm, Tokyo, Japan). The metabolically labeled Pael-R was quantified using Image Gauge software (Fujifilm).

Cell death assay

Normal HEK293 cells and those stably expressing HRD1-myc or M-HRD1-myc were transfected with a control vector or Pael-R-FLAG and incubated for 24 h. The cells were washed with phosphate-buffered saline (PBS) and then stained with crystal violet (0.1% crystal violet, WAKO Pure Chemical Industries, Osaka, Japan), and the wells washed with water and air-dried. The dye was eluted with water containing 0.5% SDS, and optical density was measured at 590 nm.

